UNIVERSITY OF OKLAHOMA

GRADUATE COLLEGE

A MICROSCOPY SCANNING SYSTEM FOR CLINICAL CHROMOSOME DIAGNOSTICS

A DISSERTATION

SUBMITTED TO THE GRADUATE FACULTY

in partial fulfillment of the requirements for the

Degree of

Doctor of Philosophy

By

MARC CONAN WOOD
Norman, Oklahoma
2007

Downloaded from SHAREOK. Persistent Handle URL: https://hdl.handle.net/11244/1264

UMI Number: 3283865



UMI Microform 3283865

Copyright 2008 by ProQuest Information and Learning Company.
All rights reserved. This microform edition is protected against unauthorized copying under Title 17, United States Code.

ProQuest Information and Learning Company
300 North Zeeb Road
P.O. Box 1346
Ann Arbor, MI 48106-1346

A MICROSCOPY SCANNING SYSTEM FOR CLINICAL CHROMOSOME DIAGNOSTICS

A DISSERTATION APPROVED FOR THE
SCHOOL OF ELECTRICAL AND COMPUTER ENGINEERING

BY

_____
Hong Liu, Ph.D.

_____
Sam Lee, Ph.D.

_____
Tamer S. Ibrahim, Ph.D.

_____
David W. Schmidtke, Ph.D.

_____
Shibo Li, M.D.

©Copyright by MARC CONAN WOOD 2007
All Rights Reserved.

ACKNOWLEDGEMENTS

I would like to give special thanks to Dr. Hong Liu, without whose encouragement and support I would not have been able to complete the Ph.D. program.

Dr. Shibo Li of the Oklahoma University Health Sciences Center was the originator of the idea for the chromosome scanning project, and has been an invaluable source of technical expertise throughout its development.

Dr. Yuhua Li provided essential technical and logistical support for the project and his friendship made the work much more enjoyable.

Xingwei Wang provided valuable assistance in software and image processing ideas.

Funding for this study was made available by the National Institute of Health.

TABLE OF CONTENTS

	PAGE
Acknowledgements	iv.
Table of Contents	v.
List of Tables	vi.
List of Illustrations	vii.
Abstract	ix.
Chapter I. Chromosome Diagnostics	1
Section 1.1 Introduction	1
Section 1.2 Structure of Chromosomes	3
Section 1.3 Nature and Signs of Leukemia	7
Section 1.4 The Process of Mitosis	13
Section 1.5 Analysis of Tissue Slides	15
Section 1.6 Status of Research in Chromosome Scanning	17
Section 1.7 Most Important Features of a Scanning System	30
Section 1.7.1 Rapid Scanning	32
Section 1.7.2 Affordable System Cost	33
Section 1.7.3 Video Image Quality	36
Section 1.7.4 Accurate grading of metaphase cells	37
Section 1.7.5 Accurate karyotyping of chromosomes	39
Section 1.7.6 Minimal lab space requirements	40
Section 1.7.7 Minimal operator intervention	40
Section 1.7.8 Installed on lab's own computer and microscope	42
Section 1.7.9 Minimal training requirements	42
Section 1.7.10 Flexible selection of imaging options	43
Chapter II Automated Microscope Scanning Hardware	44
Section 2.1 Introduction	44
Section 2.2 Motorized Stage Design	49
Section 2.3 Video Camera	53
Section 2.4 Scanning Methods	58
Section 2.5 Determination of Microscope Resolution	64
Section 2.6 Measuring the Modulation Transfer Function	70
Chapter III Motion Scanning of Metaphase Spreads	96
Section 3.1 Visual Appearance of Scanned Metaphases	96
Section 3.2 Metaphase Finding	102
Section 3.3 Stage Coordinate Repeatability	111
Section 3.4 Summary	112
Chapter IV – Conclusion	114
References	116

LIST OF TABLES

PAGE

Table 1.1 – Scanning System Goals 32
Table 2.1 – Hardware Performance Goals 44

LIST OF ILLUSTRATIONS

PAGE

Figure 1.1 – Chromosomes in Metaphase. 4
Figure 1.2 – Depiction of a reciprocal translocation 8
Figure 1.3 – Karyotype of normal male chromosomes 9
Figure 1.4 – Karyotype showing translocation. 10
Figure 1.5 – Karyotype showing both hypo and hyperdiploid chromosome. 10
Figure 1.6 – Karyotype showing hypodiploidism. 11
Figure 1.7 – A karyotype indicating a poor prognosis for recovery. 12
Figure 1.8 – Phases of Mitosis. 14
Figure 2.1 – Diagram of Microscope Scanning System. 45
Figure 2.2 – Photo of Microscope Scanning System. 46
Figure 2.3 – A camera CCD detector layout. 55
Figure 2.4 – Semiconductor CCD pixel detector. 56
Figure 2.5 – Relationship between pixel size and pixel pitch. 57
Figure 2.6 – Diagram of slide areas. 60
Figure 2.7 – Pixel values for 20 μm segment of stage micrometer. 61
Figure 2.8 – Metaphase with micrometer scale superimposed. 62
Figure 2.9 – USAF 1951 Optical Resolution Target. 72
Figure 2.10 – Image of a stage micrometer slide. 75
Figure 2.11 – Theoretical MTF curves. 79
Figure 2.12 – USAF target with motion blur. 80
Figure 2.13 – MTF for three scan rates with 10X objective. 84
Figure 2.14 – USAF target still image with 10X objective. 85
Figure 2.15 – USAF target with 1mm/sec scan and 10X objective. 86
Figure 2.16 – USAF target with 2mm/sec scan and 10X objective. 86
Figure 2.17 – MTF for three scan rates with 20X objective. 87
Figure 2.18 – USAF target still image with 20X objective. 88
Figure 2.19 – USAF target with 1mm/sec scan and 20X objective. 88
Figure 2.20 – USAF target with 2mm/sec scan and 20X objective. 89
Figure 2.21 – MTF for three scan rates with 40X objective. 90
Figure 2.22 – USAF target still image with 40X objective. 91
Figure 2.23 – USAF target with 1mm/sec scan and 40X objective. 91
Figure 2.24 – USAF target with 2mm/sec scan and 40X objective. 92
Figure 3.1 – Metaphase image scanned at 2 mm/sec using 10X objective. 97
Figure 3.2 – USAF target scanned at 8 mm/sec using 10X objective. 98
Figure 3.3 – Still image of metaphase using 10X objective. 99
Figure 3.4 – Still image of the center metaphase using the 60X objective lens. 99
Figure 3.5 – Image captured with 1mm/sec scan rate. 100
Figure 3.6 – Image captured with 2mm/sec scan rate. 100
Figure 3.7 – Image captured with 1mm/sec scan rate and 60X lens. 101
Figure 3.8 – Image from Figure 7.5 captured at 2mm/sec scan rate. 102
Figure 3.9 – The 21 x 21 window segmenting a metaphase. 105
Figure 3.10 – Pixel values for binary metaphase window. 106

Figure 3.11 – Co-occurrence matrix for **d** = (1,1). 106
Figure 3.12 – Still image containing four candidate metaphases. 109
Figure 3.13 – Result of finder process. 109
Figure 3.14 – Scan image of same tissue area. 110
Figure 3.15 – Results of finder process. 110
Figure 3.16 – Metaphase repeatedly located by software command. 112

ABSTRACT

An important part of the diagnosis and treatment of leukemia is the visual examination of the patient's chromosomes. Chomosomal changes serve as indicators of the nature and severity of the disease. Clinical genetics laboratories acquire images of metaphase chromosomes using a microscope and camera system, usually by manual search of the tissue slides. Manual techniques are labor intensive, slow and costly. A computer controlled scanning system can be an important tool for automating and expediting the chromosome analysis process. Commercial systems have been developed, but fall short of providing an automated (or even semi-automated) computer aided diagnosis technique. This dissertation describes the design and development of a prototype scanning system, and studies the impact of the scanning speed on the image quality, with an eye towards the development of a Computer Aided Diagnostic (CAD) system. The system consists of a laboratory grade microscope, a high-precision motorized stage, a video imaging system, and controlling software. An entire slide can be imaged and captured into a digital file for later review. Fast scan rates make a system more productive, which is essential for clinical practice, but motion blur can render the images unusable for post image processing and computer assisted diagnosis. Experimentally in this research, clinical chromosome images and resolution patterns were scanned under different objective lens magnifications ranges from 10X to 100X, at different scanning speed from 0mm/sec to 4mm/sec. These images were reviewed by observers. Significant motion blurs were observed at high magnification and scanning speed. The impact of

scanning speed was also quantified by objective parameters such as modulation transfer functions (MTF). For example, with an objective lens power of 10X, the essential structure of a metaphase spread can still be visually detected with a scan speed of 4 mm/sec, whereas at that speed, the image under 60X and higher objective power is not recognized. Accordingly, an optimal design strategy for an efficient clinical system should balance optical magnification, scanning speed, as well as the frame rate of the camera.

During the course of this research, the following papers were authored or co-authored:

1. X. Wang, B. Zheng, M. Wood, S. Li, W. R. Chen, and H. Liu, "Development and Evaluation of Automated Systems for Detection and Classification of Banded Chromosome: Current Status and Future Perspectives", *Journal of Physics D: Applied Physics*, vol 38, 2005, pp 2536-2542.
2. X. Wang, S. Li, H. Liu, M. Wood, W. R. Chen, and B. Zheng, "Automated Identification of Analyzable Metaphase Chromosomes Depicted on Microscopic Digital Images", *Journal of Biomedical Informatics*, 2007. (Accepted for publication).

Chapter I. Chromosome Diagnostics

Section 1.1 – Introduction

A very important part of the diagnosis and treatment of leukemia is the visual examination of the patient's chromosomes. The abnormalities seen in the chromosomes of leukemia patients are an indicator of the nature of the disease. This information allows a physician to determine the prognosis for the patient and the course of treatment with the best likelihood of success.

One of the earliest biomedical applications for computer vision to be explored was the automatic recognition and analysis of G-banded metaphase chromosomes. Metaphase spreads, scattered amongst the non-metaphase cells and cell debris on a microscope slide, had to be first found under low power magnification, followed by examination of the individual chromosomes under high power [1,2]. Finding the metaphase spreads by manual means is a laborious and tedious process that can consume a great deal of a clinician's time, particularly when the tissue comes from bone marrow samples where the metaphases are usually sparse. It was recognized by the early researchers that a computer controlled microscope stage, with suitable recognition software, could automate the finding process and thus free up the clinician to perform more specialized tasks. After the spreads had been found, the clinician could then use high magnification to capture an image of the chromosomes, with additional recognition software used to perform the task of karyotyping, or assigning the chromosomes to their homologue pair designation according to the so-called Denver classification system. The chromosome identification software used

the banding characteristics of the stained chromosomes to match them to images of standard chromosome data sets.

In a typical clinical setting, a genetics laboratory technician will prepare a half-dozen microscope slides containing leukemic blood cells or bone marrow cells taken from the patient. The slides will be carefully examined under a microscope until about 20 clear chromosome images are found. The cytogeneticist who evaluates the chromosomes needs a large number of clear images in order to determine the type of cancer, as well as the state of the disease (advanced or early stage). The slide examination process can be tedious, tiring, and time-consuming. It may take up to 30 minutes to examine each slide and fatigue may prolong the process over several days.

A computerized system of slide scanning automation can be a great help to the laboratory technicians. It allows them to record each slide in a digital image file in order to view the slides on a computer monitor at a later time. The viewing time on a PC monitor can be faster, more convenient, and less tiring. When combined with image recognition and processing software, the system can automatically locate the metaphases and present them for operator selection. Several types of scanning systems are commercially available that are designed to facilitate metaphase finding and/or karyotyping. However, none of them meets the clinical demand for an automatic (or even semiautomatic) Computer Aided Diagnosis (CAD) capability.

The design of such a system requires that careful attention be paid to the selection of the components, as well as the way they are used. The hardware and software components can be expensive, especially considering the limited budgets available to most clinical labs. To achieve the most effective system for the money,

the components should be well matched. For example, a good image produced by expensive microscope optics can be seriously degraded by a poor quality video system. Furthermore, full-motion scanning, while faster than tile scanning, can introduce motion blur that further degrades the image quality, and the severity of the blur worsens with scan speed and higher levels of magnification. As the image quality decreases, it becomes more and more difficult for the clinician or the software to recognize and use the features in the image. System designers and users must be able to compare the image quality of different system configurations at various scan speeds in order to choose the right components. Therefore, a method of evaluating image quality that produces objective and repeatable measurements would be very valuable. The purpose of this dissertation was to determine the most important features for a scanning system, successfully merge the appropriate hardware and software components, develop methods for critically evaluating the image quality of such a system, and demonstrate its ability to quickly and accurately scan slides for chromosome diagnostics. The results of this research will facilitate the future development of a clinically functional system.

Section 1.2 – Structure of Chromosomes

Chromosomes, from Latin meaning "colored body", are the carriers of genetic information in plants and animals. Figure 1.1 shows a set of human chromosomes, the way they appear during cell division, or *mitosis*.[1] They reside in the nucleus of a cell, and when not in the process of mitosis, they appear as tangled webs of DNA,

[1] The process of cell division in sex cells is called meiosis. This document focuses on mitosis.

called chromatin. Each chromosome is made up of one extremely long DNA molecule [31-35].

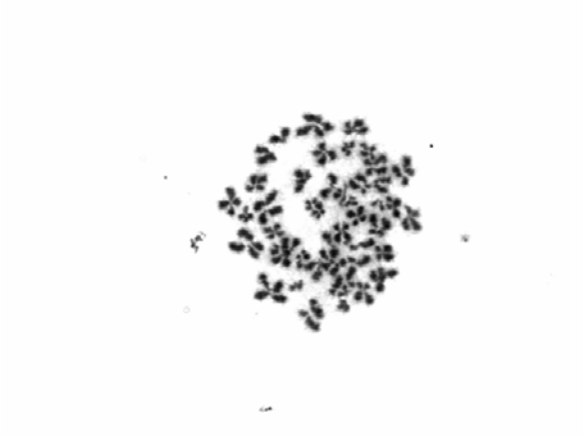


Fig 1.1 – Chromosomes in Metaphase.

If the entire molecule were to be stretched out end to end, it would be over 1 meter in length, even though in its compact form it is only about 10 μm. DNA, or deoxyribonucleic acid, is a double-stranded chain of nucleotides, with a nucleotide on one strand being complementary to the adjacent nucleotide on the other strand. A nucleotide consists of an organic base, a five-carbon sugar (pentose), and a phosphate group. There are only four kinds of organic bases in a DNA molecule: adenine(A), guanine(G), cytosine(C), and thymine(T). Each of the bases is joined to one other, forming a complementary base pair, with the two bases of a pair held together by hydrogen bonds. If we think of the chain as being like a lattice, or ladder, the base pairs are connected so as to form a "rung" in a flexible ladder that is slightly twisted into the double-helix shape discovered by Watson, Crick, and others in 1953. Another common analogy describing this arrangement is the *rod-ribbon* model,

where the base pairs are the *rods* and the sugar-phosphate backbone forms the two *ribbons*. Guanine(G) is always paired with cytosine(C), and adenine(A) is always paired with thymine(T). The structure of the molecules allows them to hydrogen bond in a complementary fashion.

A single chromosome may have hundreds of millions of these base pairs. The sequence of the bases along the chain forms a code. Certain sections of each chromosome are arranged into base pair sequences that form a unique code that specifies how the cell will perform a particular function. These sections are known as *genes*. Typically, the code in a gene is used to construct the proteins that are needed for the cell to maintain its own life, or for proteins that are needed by the organism's system outside of that cell (e.g. hormones produced by endocrine gland cells used in other parts of the body). Other sections of the DNA strands perform other roles, such as transcription of RNA (Ribonucleic Acid) molecules.

During mitosis, the strands of DNA must be *replicated,* so that each of the new cells has a complete and accurate copy of the genetic information. This is where the complementary nature of the base pairs is so effective in providing a simple means of creating the correct sequence of nucleotides along each part of the strand. At the beginning of the replication process, the hydrogen bonds holding the two bases of the pairs separate in a manner that allows the chain to "unzip" along part of its length. Then, each half of the chain becomes a template for producing a new complementary half. The fact that the bases only pair up with their complementary bases is what determines the sequence along the new chain. By the end of the replication, the entire length of the DNA molecule has been unzipped. Each of the

old strands in the chain has a new strand built onto itself to replace its old mate strand, while the old mate is at the same time getting its new complementary strand added to it. In this way, two complete double helices, known as *daughter* chromosomes, result from the replication process. Several enzymes, specialized proteins that help to catalize chemical reactions, are essential in the replication process, making it possible to unzip the chain, synthesize the new strands, and separate the strands into two independent chains.

The replication process is normally very accurate and the sequence of base pairs is copied faithfully. If errors do occur, there are enzymes that play a role in detecting the errors, then cutting out and replacing the incorrect bases. When the correction process does not succeed, sequence errors can become permanent, resulting in a genetic *mutation*. Some mutations are so severe that the resulting cell, or cells, are not viable, and die very quickly. However, others survive to maturity, then later divide into two cells, both having the same mutated DNA. In some cases, the mutation results in a benign anomaly, not causing any harm to the organism. In other cases, the cells survive but cannot perform their proper function and the organism suffers deleterious consequences. Many diseases, such a hemophilia, sickle cell anemia, and diabetes, are attributed to these genetic mutations that can be passed down to succeeding generations. While the impact on individuals is often tragic, the mutations are thought to bring about a wider good to Nature in general, making it possible for chance mutations to give an organism a lucky adaptation to a changing environment. That mutated organism may have a better chance of survival than the previously majority of individuals which did not have it, and so the mutated

individual will succeed in passing its genes on to the next generation, while those without the mutation may succumb to environmental forces and die off.

Section 1.3 - Nature and Signs of Leukemia

One of the diseases with a genetic characteristic which occurs all too frequently is leukemia. The disease gets its name from the white blood cells (*leukocytes*), which it affects [32]. White blood cells help the body fight infections and other diseases. There are forms of leukemia affecting animals other than humans, such as feline leukemia, but the disease is especially a source of great tragedy among human populations, both young and old. The disease is not passed on to offspring *per se*, though the propensity to be inflicted with the disease may be, but rather comes into existence by mutations that occur after birth. The exact cause of the leukemic mutations is not known, but exposure to environmental toxins or radiation is thought to contribute to its onset. Once cells have the mutations associated with leukemia, they reproduce rapidly and can eventually overwhelm the body with their numbers. The body's immune system tries to eliminate the defective cells, but will lose the battle over time. The disease affects the production of the blood cells that are needed to help the body fight off such diseases, making it that much more difficult for the body to eliminate the defective cells. The lymph nodes, spleen, and other organs become clogged and swollen with the defective cells and become ineffective in performing their intended purpose. If untreated, the disease is usually fatal.

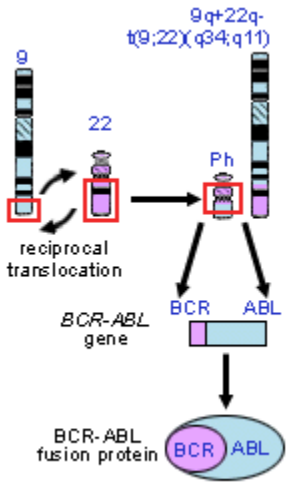


Figure 1.2 – Depiction of a reciprocal translocation. Source: National Center for Biotechnology Information. Copyright ©NCBI

There are a few types of leukemia which show common features. One of the best known is the so-called translocation, depicted in Fig 1.2. In this type, a section of one chromosome will be cut loose, and relocated to another chromosome. Because this form of leukemia was first identified at a hospital in Philadelphia, PA, it is known as the "Philadelphia Chromosome". Fig 1.3 shows a karyotype of a normal male , while the karyotype in Fig 1.4 displays the translocation anomaly.

In other cases, the karyotype contains an incorrect number of chromosomes, or an incorrect arrangement of the pairs. Fig 1.5 shows a case where there are too many chromosomes, with some of the homologous pairs containing more than two members. This condition is known as hyperdiploidism. Fig 1.6 shows the opposite case, where there are too few chromosomes, a condition known as hypodiploidism. In other cases, a combination of defects will be seen. Fig 1.7 shows such a case. The

prognosis for this individual is very poor; the disease has progressed to a point where treatment may not eradicate the defective cells.

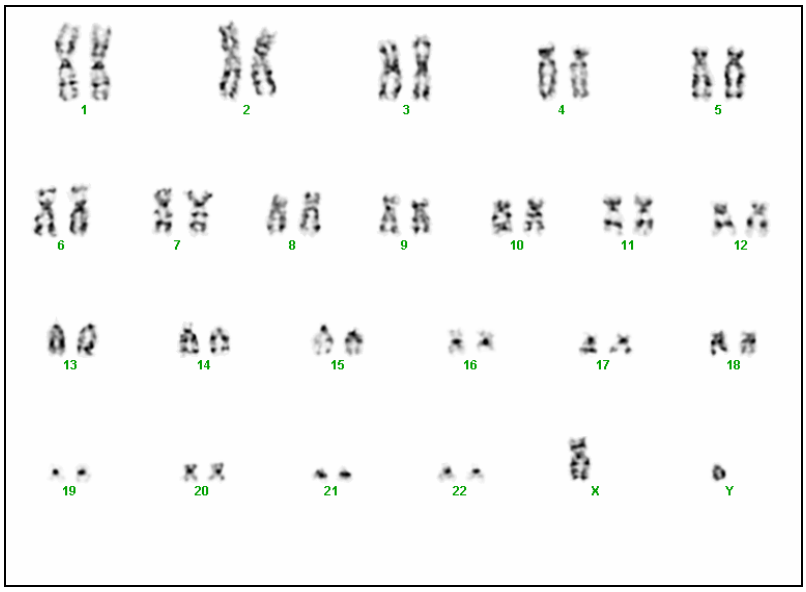


Fig 1.3 – Karyotype of normal male chromosomes

.

Normally, stimuli of a healthy biological nature cause cells to begin the process of mitosis. The cells divide at a rate which is appropriate for the age and health of the individual, with rapid growth during gestation and infancy necessary for physical development, but slower rates of division during adult years. Cancer cells, on the other hand, tend to divide rapidly. This rapid division can produce so many disease cells that the body's immune system cannot cope with the large numbers.

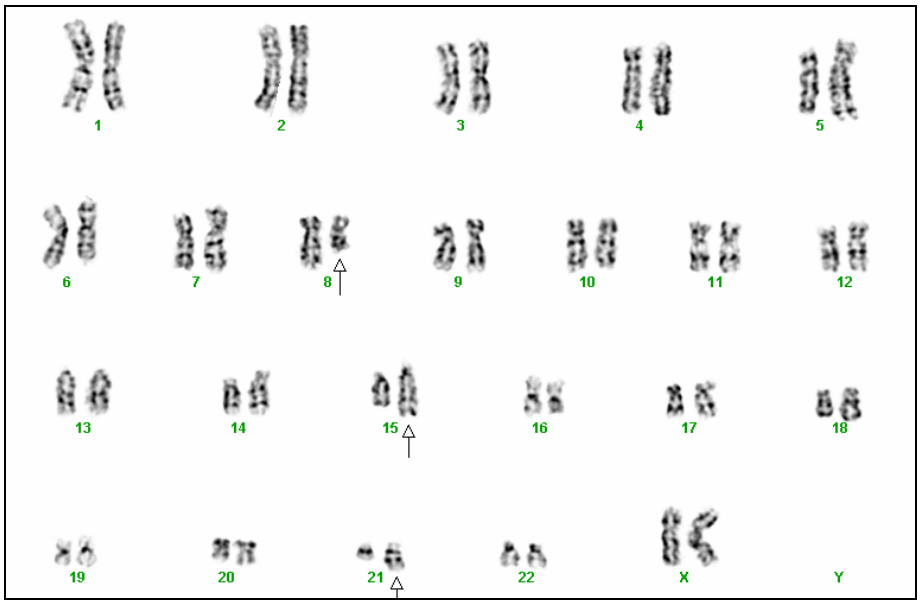


Fig 1.4 – Karyotype showing translocation.

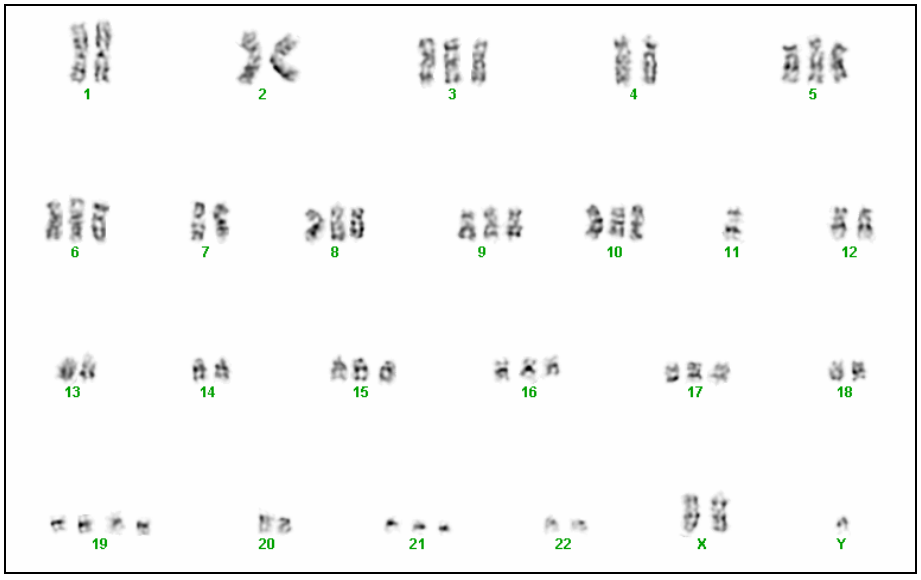


Fig 1.5 – Karyotype showing both hypo and hyperdiploid chromosomes.

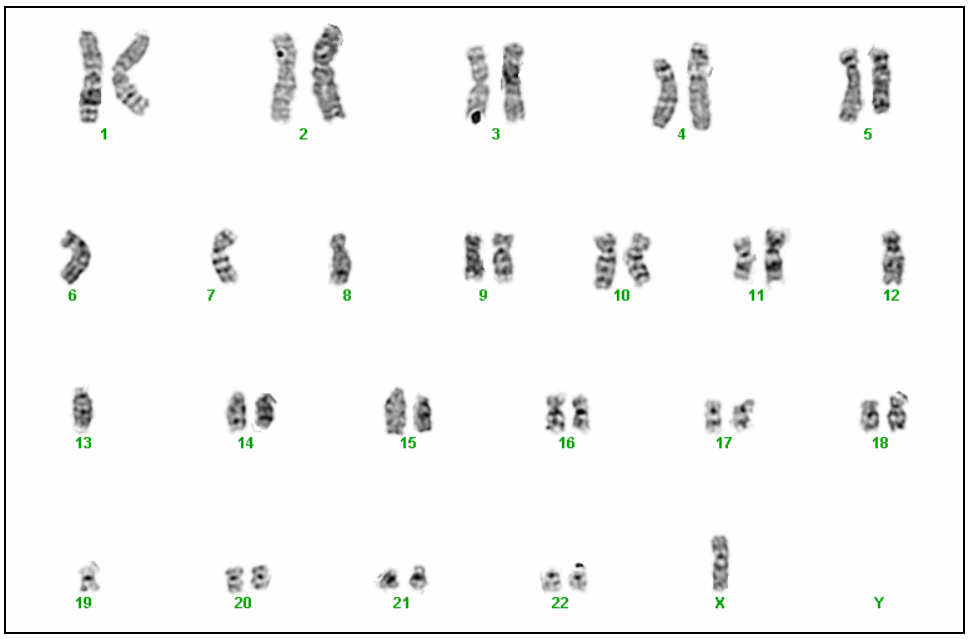


Fig 1.6 – Karyotype showing hypodiploidism

The fact that leukemic cells are dividing rapidly gives oncologists a way of fighting the disease. Chemotherapy can target cells that are in the process of dividing, while causing minimal damage to other cells. In this way, a war of attrition can be fought against the disease, wherein far more disease cells are destroyed than normal healthy cells. Even then, the pharmaceuticals used in this way often cause harmful side effects, such as loss of hair, nausea, bone degeneration, etc. The pharmaceuticals are toxic, and it is only because the disease, if left untreated, will almost certainly lead to death, that justifies introducing these substances into the body.

The toxicity of the treatments for leukemia is one reason that the prompt and accurate diagnosis of the disease is so essential. An inaccurate diagnosis, such as a

false positive, could cause a patient to unnecessarily endure the detrimental effects of the treatment. A false negative diagnosis could delay treatment to a point where only massive doses of pharmaceuticals offer any hope of recovery, bringing about side effects that may be unendurable for the patient. An incorrect identification of the type of leukemia could lead to an improper regimen of chemotherapy which could cause the disease cells to develop a resistance to the treatment, making the disease even more difficult to eliminate. The proper design and use of a microscope scanning system could play a very beneficial role in improving the safety and effectiveness of a treatment program.

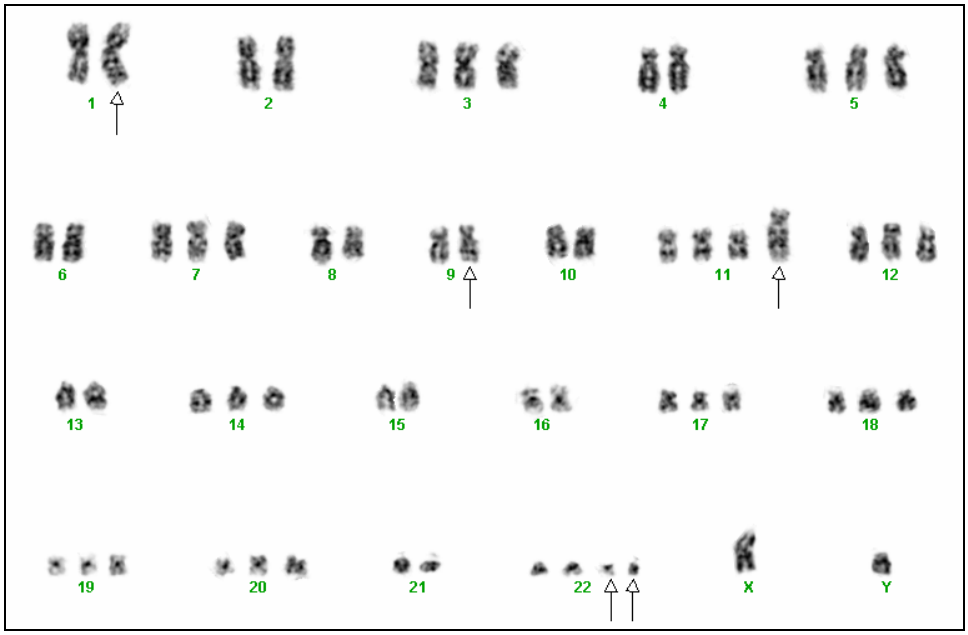


Figure 1.7 – A karyotype indicating a poor prognosis for recovery

Section 1.4 The Process of Mitosis

Cell division is also of major interest to the cytogeneticist because it is only during mitosis that the DNA condenses into the individual bodies that we recognize as chromosomes [35]. Diseases like leukemia cause characteristic abnormalities in the chromosomes which are impossible to see when the DNA molecules are jumbled up into the mass of chromatin that normally resides in the nucleus. The abnormalities seen in the chromosomes are vital clues in understanding the nature and severity of the disease. Figure 1.8 shows the individual stages of cell division. During most of a cell's existence, it is in the *interphase*, where it is performing its normal functions; in this state, it is impossible to tell one chromosome from another or detect abnormalities. The division process starts with the *prophase*, where the chromatin begins to condense into the characteristic chromosomal shape. The centrosomes move to opposite sides of the cell and the nuclear envelope breaks down. The spindle apparatus appears, attached to the centrosomes. The chromosomes replicate, with the two new helices being called sister chromatids. During *metaphase*, the sister chromatids become attached to the spindle fibers and migrate to the center of the cell, aligning themselves along the equator. Then, the spindle fibers pull the sister chromatids away from each other, with a complete set going toward each centrosome. The cell is now in *anaphase*, and the entire cell begins to divide into two separate and complete cells, each having a complete set of chromosomes which should be exact duplicates of the original DNA that existed before the process began. In the last step of mitosis, the *telophase*, two completely separate cells exist, with each one

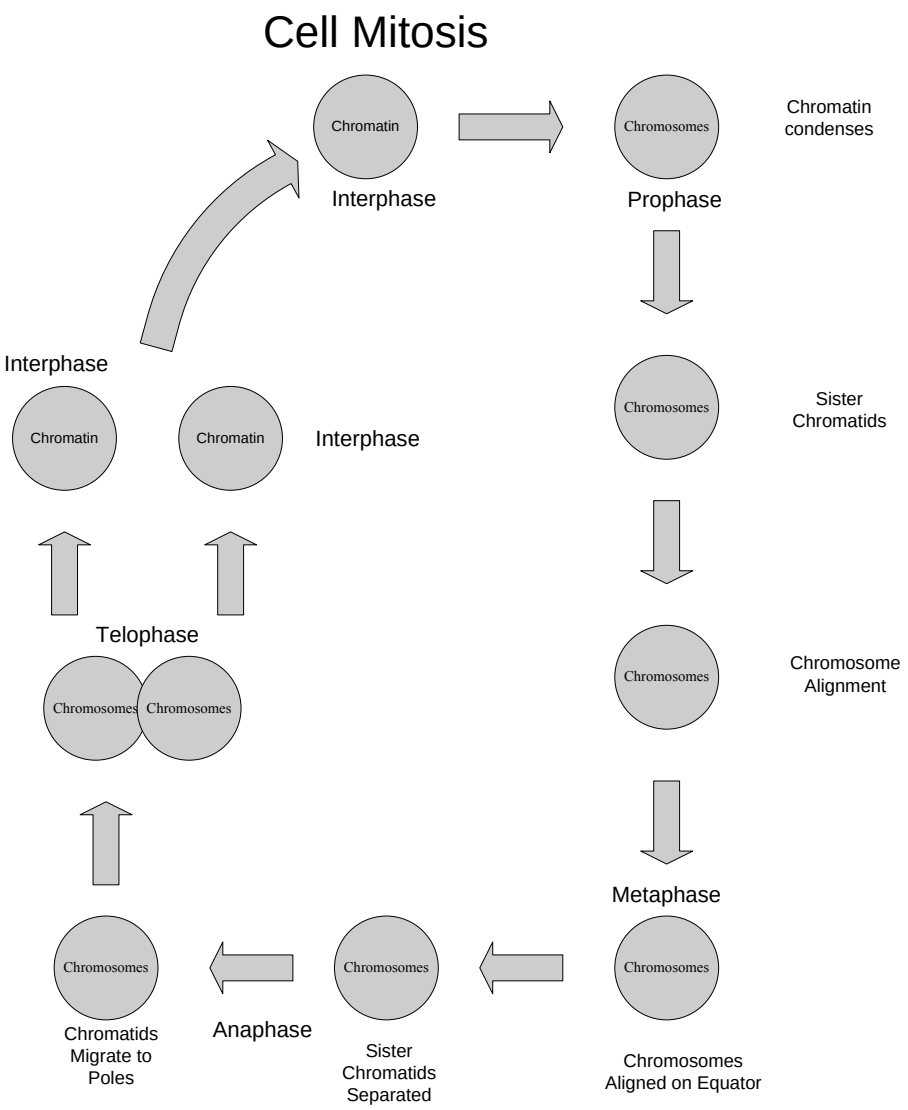


Fig 1.8 – Phases of Mitosis

reforming its nuclear envelope with the vital structures enclosed. The cells then return to the interphase, with their tangled mass of chromatin holding the genetic information.

Section 1.5 – Analysis of Tissue Slides

Since the chromosomes are distinctly visible only during the metaphase, it is desirable to obtain an image of them during this part of mitosis. At this point, the chromosomes are referred to as *metaphase chromosomes*. Cytologists have developed specialized techniques, called *protocols*, for imaging the metaphase chromosomes [31,32]. For leukemia diagnosis, blood and bone marrow samples are taken from the patient during a biopsy. The samples must be transferred to microscope slides so the chromosomes can be clearly seen. Immediately after the biopsy, the cells are cultured in a pH and temperature controlled medium which contains nutrients to sustain the cells. Antibiotics are added to prevent the growth of bacteria. In order to see as many cells as possible in metaphase, the clinical technician will apply antigens to the sample to induce the cells to divide. This action increases the proportion of cells that move into mitosis, providing a better chance that the chromosomes will be viewable. After about 24 hours of cell division, a chemical is added to the tissue that arrests the cells in metaphase. This has the effect of "freezing" the cells in a state where their chromosomes are visible and aligned in pairs.

After the mitosis process has been halted, the tissue is treated with another chemical which causes the cells to *lyse*, or rupture, allowing the chromosomes to come out of the nucleus and the cellular material to separate from the chromosomes. At this point, the cells are no longer alive. The material is then dropped onto microscope slides, stained with Giemsa stain, and allowed to dry. The stain is absorbed by the chromosomes, causing them to appear dark under the microscope.

The tissue from one patient will be used to prepare five or six slides. Once the slides are dry, they are examined under the microscope, using a dry objective lens of approximately 10X magnification. The lab technician searches the slide for useful chromosome images. A good image will show all the chromosomes from a single cell in a small circular group, without chromosomes touching, overlapping, torn, or folded. A well-prepared slide will have relatively little cell debris so that there is less chance of the chromosomes being hidden underneath other material.

The goal is to find, among the five or six slides prepared, approximately 20 good quality images that the cytogeneticist can analyze. The choice of objective lens to use for this stage of the chromosome analysis is based on visualizing the chromosomes clearly, and to reduce time spent on the searching process. A higher level of magnification would greatly increase the time required to search the slides. Furthermore, an extremely high level of magnification usually requires an oil lens, which is not suitable for searching an entire slide. The high magnification oil lens is used later on for detailed examination of the individual chromosomes during the process of *karyotyping* (assigning each chromosome to a numbered pair).

The cytogeneticist or laboratory technician will place the slides individually in the slide holder mechanism on the stage. Next, the illumination and focus are adjusted to obtain a clear image of the metaphases and other cell bodies. The condenser lens should be adjusted for Kohler illumination. He or she will operate the microscope stage manually by turning the two knurled knobs that move the stage in the X and Y axis so that the entire slide is carefully searched for metaphases. After a metaphase is found, it is usually examined under higher magnification, such as 60X

objective power, in order to determine if it is a "good" metaphase, meaning that the chromosomes are clearly imaged, with minimal overlap. It is usually easier to find good metaphases when viewing blood cell chromosomes, whereas bone marrow cells generally provide fewer good metaphases. After a good metaphase is found, its XY location is determined by removing the slide and replacing it with a standard slide that is divided up into labeled grids. The grid number that appears in the eyepiece is used as the grid location of the metaphase that was just found. This is step adds time to the process, and can easily be eliminated by using a motorized stage.

As metaphase images are chosen, their slide ID number and XY coordinates are recorded for later review. After 20 good quality metaphase images are located on the slides, the images can be located and recorded into a digital image using a microscope camera and appropriate imaging software.

Section 1.6 - Status of Research in Chromosome Scanning

Beginning in the 1960s, image recognition researchers began to formulate the fundamental ideas of recognizing metaphase spreads and individual chromosomes [1-3]. In the 1970s, researchers in the field of chromosome scanning, including Neurath, Mendlesohn, Castleman, and Piper extended the work, and a number of important papers were published on the subject [21]. As the need for cytogenetic analysis has increased over the years, serving both geneticists, oncologists, and other scientists, the desirability of an automated chromosome analysis system has greatly increased.

Prior to computer assisted methods, cytogeneticists would manually locate the metaphase spreads under low magnification, an approach still used in many laboratories. They then used conventional film cameras to capture the metaphase spreads under high magnification. The film would be developed in a nearby darkroom, and the individual chromosomes separated by cutting the film with scissors. The chromosomes could then be taped or glued to a sheet of paper to form a karyogram, with the chromosome pairs labeled. The karyogram could then be re-photographed to form a permanent record of the patient's diagnosis. Some early computer systems were little more than "electronic scissors" [12], allowing the chromosomes to be separated, or "segmented" with a light pen, mouse, or other pointing device. This process has been considered long, difficult, and boring, making it a good candidate for computer assistance. By 1972, there was optimism that the automated systems were being perfected and would soon be a truly successful application of pattern recognition [11]. The great difficulties that lay ahead in solving the practical problems of these systems were not wholly appreciated at that time. Some of these problems are still with us today, 35 years later. The software algorithms required to classify chromosomes are still an area of great difficulty, mostly due to the variability in the appearance of the chromosomes in the typical clinical microscope image.

The research continued throughout the 1970s, aided by improvements in optical instruments and computers. Important research institutions included JPL, Western General Hospital in Edinburgh, Scotland, and Tuft's Hospital. By 1978, the essential functionality of an automated chromosome diagnostic system had been

thoroughly described, and Castleman and his associates, working under a NASA contract, filed a U.S. patent on the system [7]. The following is quoted from the abstract of the patent:

Automated clinical system for chromosome analysis
Abstract

An automatic chromosome analysis system is provided wherein a suitably prepared slide with chromosome spreads thereon is placed on the stage of an automated microscope. The automated microscope stage is computer operated to move the slide to enable detection of chromosome spreads on the slide. The X and Y location of each chromosome spread that is detected is stored. At the conclusion of this searching operation, the computer directs the microscope to again sequence through the chromosome spread locations in response to the stored X and Y locations. At this time an operator can view these spreads to determine which ones are worthwhile and which ones are not. He is provided with an accept-reject switch. The microscope stage thereafter again sequences through only the accepted chromosome spreads, and this time a digital photograph of each of the chromosome spreads is made and entered into the computer storage. The computer thereafter measures the chromosomes in a spread, classifies them by group or by type and also prepares a digital karyotype image. This image is converted to analog form, displayed and printed out and constitutes a primary output of the system. Chromosome measurement data is filed in an interactive data base for subsequent statistical analysis. The computer system

can also prepare a patient report summarizing the result of the analysis and listing suspected abnormalities.

The ultimate usage of such a system has expanded somewhat since 1978. For example, it may be desirable that a chromosome scanning system should be connected to a Picture Archive and Retrieval System (PACS) for a permanent record of the slide images. PACS are becoming more and more common today, whereas they may have been only a subject of speculation in 1978 (See [51] for a description of PACS) . And, while there have been great strides made in optics, computers, and stage control circuitry, the functionality of the systems that are commercially produced today are essentially the same as described in the Castleman patent.

An important update to the status of the research appeared in the literature in 1980 [8]. In this paper, Piper, described the operation of a scanning system; and reported on the results of experiments conducted at his facility compared with those being reported elsewhere in the literature at that time. The typical system used a minicomputer to perform the pattern recognition functions, with custom hardware used in some cases to threshold the images prior to processing. Experiments with parallel processing were already being conducted in an attempt to improve the throughput of the system. Vidicon television cameras were often used in early experiments, with the stage moved in a start-stop motion whereby the slide was captured as a series of tiled subimages. This approach was quite slow, but improvements had reduced the scan time to 15 minutes. Continuous scan systems, on the other hand, used CCD arrays. The CCD array camera scanned a strip of the slide perpendicular to the direction of the stage movement. In this method, the image was

captured in a back and forth motion, with adjacent strips scanned in opposite directions. These two methods of scanning still have their advantages and disadvantages, and both are still in use.

The Piper paper described the various attempts at recognizing chromosomes, by size, shape, and the banding patterns. The metaphase finders, which processed low magnification images to find the metaphase spreads, typically used morphological techniques, such as dilation and erosion, to separate the spreads from cell debris and other objects on the slides. Size and shape measurements were then used to further reduce the number of candidate objects, after which texturing methods could make a final classification. Coherent optical systems were also tried as a means of deriving a Fourier transform of the image in real time, and the transform being used to detect the frequency spectrum associated with a metaphase spread. With the advent of fast digital signal processing hardware and software, obtaining a Fourier transform digitally is far easier today than in 1980, so the optical approach may not have the advantages that it once did.

Various digital image processing techniques were described by Nickolls, Piper and other researchers in the 1980s. Gaussian filters, Fourier decomposition, statistical analysis, fuzz logic, and neural network approaches were being tried. The literature often reported "encouraging results" in these attempts to recognize and classify the chromosomes, but the false positive and false negative rates were still too high to make the systems appropriate for a clinical setting. Piper reported that metaphase finders were being developed for commercial sale, but still being plagued with high error rates, had not been released for clinical use in. Because metaphase finding can

be performed by a clinical technician with only moderate skills, laboratories then, as now, felt that an automated metaphase finder would need to be relatively inexpensive to be cost effective.

After Piper's landmark paper, other researchers reported their findings and results. In 1981, Nickolls, in collaboration with Piper and others, reported on research to develop chromosome recognition methods [9]. This important paper focused on the image preprocessing designed to improve the results of the recognition algorithms being tried. It had already been found that variation in the quality of the images had a significant impact on the success of the recognition algorithms. While the chromosomes on one slide might be recognized with satisfactory error rates after the algorithm was adjusted, the same adjustments did not work well for the images taken from another slide, and so the algorithm's parameters and limits would have to be adjusted all over again. Various kinds of digital filters were tested, with the purpose being to enhance or accentuate features being used for segmentation and recognition, while reducing image noise. Then, as now, consistent contrast was extremely important for improving the accuracy of pattern recognition. This research attempted to develop means to improve contrast for those specific features which were to be used for the segmentation and recognition steps. These preprocessing steps required a great deal of CPU time with the computers available in 1981. Even though computers are much faster today, and dedicated hardware using DSP technology could be used to speed up the process even further, improvement of image quality is still best done at the optical level, where better microscopes and cameras can greatly improve contrast in an instantaneous manner.

In the years since Piper's 1981 paper, experience with digital preprocessing has shown that feature enhancement and noise filtering usually work at cross purposes. Any attempt to remove noise as a means of improving the signal-to-noise ratio will result in smoothing the edges, thus blurring those features that are needed to perform segmentation and classification tasks [44]. Again, preprocessing time was a significant drawback to this approach. In 1983 Castleman reported on efforts to speed up the processing by using a pipeline multiprocessing architecture [10].

By the mid 1980s, researchers had gathered significant clinical experience with scanning and classification [11,12,13]. In 1986, Lundsteen and his associates reported on a 16 month study, started in 1983, of the use of a semi-automated karyotyping system at The University of Copenhagen. They reported an error rate of 8-9%. Their system used a specialized image processing system called Magiscan 2. A motorized stage and video camera captured the microscope images and fed them to the Magiscan 2 for processing. Magiscan 2 controlled the light source intensity, the stage movements and the microscope focus (Z axis) motors. Built in image processing code allowed for efficient (in 1986 terms) analysis of small regions of an image. Metaphase finding was said to be performed in a completely automatic fashion by Magiscan 2. For chromosome classification, density profiles were used to form most of the feature set, while centromeric index and other factors formed an eleven-dimensional attribute vector for each chromosome. Using statistical methods to calculate the maximum likelihood values, chromosomes were assigned to the karyotype. An operator, using a light pen, interacted with the software to make a final determination of the correct karyotype.

This paper mentioned a difficulty which still plagues segmentation and classifications schemes, that bent or overlapping chromosomes often result in an incorrect classification. Even if a segmentation of overlapping chromosomes is done correctly, at least one of the chromosomes is likely to be misshapen afterwards. Bent chromosomes cannot be easily straightened out. Lundsteen removed these cases from the data set in order to concentrate on the more basic tasks of classification, something that is impractical in a clinical setting. Furthermore, this paper pointed out another prevalent problem, which is that classifiers work fairly well when tested against their own training data set, but not nearly as well against an unrelated training data set. This fact highlights one of the most challenging aspects of clinical use, which is that most uses of a chromosome analysis system would be for identifying abnormal chromosomes, which would comprise a data set with significant variation from the standard training, or even testing, data set.

In 1987, Graham and published a two-part study of automated chromosome analysis, also using the Magiscan 2 system [12,13]. Part I pertained to chromosome segmentation and classification, while Part II covered metaphase finding. This implementation was a highly interactive system, with the operator using a light pen to correct mistakes in the segmentation and karyotyping. Images were preprocessed with a global histogram method in order to adjust for lighting conditions. Medial axis, density profiles, and centromeric measurements were used as features in the classification steps. Error rates of 2% to 8% were reported, depending on the variance of the test data set. Variability in slide preparation quality in an actual clinical environment is almost certain to make the error rates worse.

Graham pointed out a difficulty in the clinical use of these systems in the 1980s; namely, that a cytotechnician "cannot in general be expected to have much interest in (or sympathy for) computers". Hopefully now, 20 years later, all laboratory technicians are quite familiar with computers and no longer have objections to using them. Still, today's technicians cannot be expected to achieve high productivity with a system unless it represents a substantial improvement in methodology, compared to traditional manual methods. After all, the goal is to obtain a diagnosis as quickly as possible, with minimum difficulty and high reliability, and the system must help achieve that to be considered an asset. Only about one-third of the samples processed in the hospital where the study was conducted were processed using the Magiscan 2 system. The others were performed manually. Graham concluded this paper by pointing out that the number of interventions required by the technician to obtain a correct karyogram was excessive (46 on average). As has been pointed out in other places in the literature, if a system requires excessive interactions, then it serves as little more than "electronic scissors".

In Part II, Graham discussed the metaphase finding part of the system, which also ran on the Magiscan 2. It was pointed out that a metaphase system must be affordable because, even though manual searching is tedious and time consuming, the cost is relatively low if a technician of moderate skill is employed for that purpose. The finding scheme performed preliminary searching using a second derivative texture operation over a 32 x 32 pixel box. If a box measured above a texture threshold, it then used morphological open and close operations to eliminate objects of the non-metaphase size and shape, and relied on a count of the number of objects

within a candidate metaphase to make a final determination. Lastly a trapezoidal merit function assigned a "grade" to the metaphase, so as to assist the operator in determining which metaphases to examine further. He stated that previous researchers had used gray level thresholding, but the texture method was more robust across different samples. The finder used autofocus, based on a proprietary algorithm (not described) applied across the slide, in order to reduce variability in the appearance of the chromosome features. One key aspect of metaphase finding is that, as a box, or window, of pixels are examined, the entire window is not recomputed with each movement of the box. Only the new pixels, in a vertical line, are calculated, throwing away the pixels that left the box; and the results being saved for the next box. In this way, computation time is greatly reduced. The recognition algorithm used should be specifically written to take advantage of this idea. Another important feature is that scanning stops as soon as some minimum number of "good" metaphases are found on each slide, or on a set of slides if a multi-slide stage is used.

Graham reported that scanning took a lot of time. He stated, however, that speed was not important because the scanning was done unsupervised at night, when the time consumed did not interfere with productivity. The research showed that in a clinical setting, the false positive and negative rates are correlated to the relative abundance of good metaphases. With blood samples, good metaphases are common, so the false positive rate is low (3%). With amniotic fluid, good metaphases are less abundant, and the false positive rate is higher (30%). The false negative rate was fairly high for both types (30- 40%). The study did not include bone marrow samples, where good metaphases are even less abundant. These rates were achieved

with a magnification power of 160X. In order to improve the accuracy of the finder when searching amniotic samples, the magnification had to be increased to 256X, thus providing higher resolution and more accuracy when counting the number of objects in the metaphase spread. Higher magnification requires more searching time because of the smaller field of view; however, Graham stated that the scheduling of the search at night rendered this problem a moot point.

Research continued in the late 1980s, with many experimenters attempting to use neural network [17] and fuzzy logic [18] approaches to chromosome classification . The expert systems approach was another idea. In 1987, Castleman [19] presented requirements for the user interface for an automated system. Piper in 1989 reported on success in locating the centromere and axis of banded chromosomes [15].

In 1989, van Vliet, et al, reported on a system dubbed "Athena", built around a Macintosh computer [14]. It was an interactive system, using what was probably the best small graphics computer of the day, operating at a 16 MHz CPU clock rate. The authors noted that at the time of their writing, there were at least 10 companies already marketing chromosome analysis systems, with varying levels of capabilities. The Athena system allowed an operator to choose the types of filters and morphological operations to use for each metaphase, and to also select various statistical parameters for forming the classification process. The classification scheme centered around measurements of centromeric index and band parameters, with *a priori* probabilities used to determine class. The time to accomplish a karyotype ranged from 2 minutes to 6 minutes, but the average number of

interventions was excessive. Error rates for a standard chromosome database were 2 – 10%, depending on the data set used and the specific method used to measure the band parameters. No provision for metaphase findings existed in the Athena system. The authors acknowledged that the error rates were optimistic, compared with rates expected for actual clinical use.

In a second paper a year later the same authors reported on the performance of the system over the previous year [20]. This paper provided a number of screen dump images to more clearly illustrate the interactive karyotyping process. Of interest in this study was a table of the times required to complete a karyogram. It was found that 75% of the time was consumed by operator intervention, while only 25% was computer run time. Furthermore, the authors stated findings similar to what other researchers had found, which is that classification errors will greatly increase if the chromosomes are bent, misshapen, touching or overlapping, or if the image characteristics vary from image to image. Clearly, for these systems to be highly valuable, the percentage of time spent in operator intervention must be substantially decreased, and the classification schemes have to be more independent of image variability.

In the 1990s, some improvements were made in the various analysis tasks. In 1992 Castleman reported on an automatic metaphase finder (AMF) manufactured by Perceptive Scientific Insturments, Inc. The finder was a robot-equipped hardware system that, according to the report, provided good performance and reliability. The system was specialized for the different types of tissues being searched. The search required 10 minutes per slide, and was designed to handle sixty slides in ten hours.

For blood cells, an 80% success rate was claimed, with less than 20% false positives. No figures were provided for bone marrow cell finding.

The number of papers published in the 1990s, and since 2000, on analysis systems appears to have decreased. Classification algorithms continued to be an active area of experimentation, but research centered around hardware and metaphase searching methods decreased. See Wang, et al [26], for a recent review of the status of segmentation and classification research.

Today, a number of commercial metaphase finding and classification systems are available. The cost of these systems is substantial, with software being the majority of the cost. One system was recently quoted at $180,000, a substantial investment for a cytogenetics lab. The vendors of these systems generally claim excellent performance, with metaphase finding taking less than 10 minutes per slide. Robotic slide handlers and multi-slide stages are usually used to obtain high throughput. A recent article [28] by Aperio Technologies Inc. claimed high accuracy in advanced scanning capability, using line scanning with an array detector, and ultra-precise linear encoders for the motors that provide highly accurate determination of stage position, even when moving continuously. It should be noted that if a stage moves at a constant speed, the position of the stage will be well synchronized to the camera frames, allowing the position of each metaphase to be accurately determined with an accuracy of a few microns. However, if the speed is not constant, this synchronization is not perfect, and the position may not be determined properly. The Aperio technology is advertised to eliminate that problem. The system is a specialized piece of hardware, with a built-in optical system.

The Metafer metaphase finder, manufactured by MetaSystems, Inc., is advertised to scan in under 6 minutes per slide. It interfaces to the MetaSystems Ikaros interactive karyotyping system, which the company advertises as being "ingenious". The system is said to be able to perform karyotyping on the most common types of staining or fluorescence. It offers a large suite of image processing tools for image handling, including enhancement, storage, etc. It appears that the operator would need to have some level of imaging skill in order to use the tools effectively. While the metaphase finder is advertised as automatic, the karyotyping function is not; it is interactive. Metaphases are presented to the user with a score which rates the potential usability of the metaphase for karyotyping. A recent journal article by Wang, et al, reported on a new technique for grading metaphases for analyzability [27].

The systems that are commercially available today are very expensive, and cannot be considered to be automatic. A cytogenetics laboratory would have to determine for itself whether the high cost of the system is an efficient use of their operating budget. Many of the same image quality problems still plague these systems today, just as they did in the 1970s and 80s. Despite the enormous amount of research put into classifier algorithms and methods, and great improvements in optics, variability in image characteristics still weakens the performance of the karyotyping schemes. Much more work will need to be done on the software in the future. Perhaps a future finding in psychophysics, whereby the function of the human brain's visual system is better understood, will be the key to discovering a whole new way of performing chromosome analysis.

Section 1.7 – Most Important Features of a Scanning System

In order to design a successful scanning system, it is helpful to establish features that describe what the system should be able to do. These specifications can then be used as design guidelines to help keep the project on track. The specifications should always be written with cooperation of those expected to be the users of the system, namely, the cytogenetics labs that perform diagnostics on the chromosomes taken from a patient. For this project, the help of the Pediatrics Genetics Lab at the Oklahoma University Health Sciences Center was asked to provide a ranking of the most desirable features that they would want to see in such a system. This section will describe those features and discuss the design challenges that can be expected when trying to satisfy the requirements.

Table 1.1 shows the chosen features in rank order of importance. The table shows the measurement goal for each feature, along with what the project was able to achieve, and whether or not the goal was met. Some of the goals are deferred until the 2nd phase of the project, the software part, which is nearing completion. This section of Chapter I will describe these features and explain the table.

Feature	Goal	Achieved	Goal Met Y/N ?
Rapid Scanning	Less than 30 min	15 min	Y
Affordable Hardware Cost	Less than $50K	$22K	Y
Video Image Quality	200 lp/mm at 10X	225 lp/mm	Y
Accurate evaluation of found metaphases	80% Analyzable	Deferred	N/A
Accurate karyotyping of chromosomes	90% Accurate	Deferred	N/A
Minimal lab space requirements	Less than 15 sq ft	14 sq ft	Y
Minimal operator intervention	Less than 5 min per karyotype	Deferred	N/A
Installed on lab's own computer and microscope	Stage Adapter and Windows PC	Stage Adapter and Windows PC	Y
Minimal training requirements	Two days training class	Deferred	N/A
Flexible selection of imaging options	Menu driven options	Deferred	N/A

Table 1.1 – Scanning System Goals

Section 1.7.1 – Rapid Scanning

For a scanning system to be truly valuable, it must complete the sequence of events quickly. Otherwise, the throughput will be too low to be worth using it. If lab workers can complete the process in the same amount of time as the automated system, and the workers are paid a modest wage, it may cost less to hire and train a person to perform the task. Working with the OUHSC genetics lab personnel, it was determined that a technician can search one slide in about 30 minutes, using a 10X

objective and a 10X eyepiece. In that time, four to six clear useable metaphase spreads need to be found and the XY location recorded. After six or seven slides are examined for each patient, the lab will have a total of 20 to 40 metaphases to use in performing the karyotyping task. The task is relatively easy with blood cell samples, but much more difficult with bone marrow samples, where the metaphases tend to be more sparse. For a computerized system to do the searching and identify the metaphases on one slide, a time of 5 minutes per slide would be considered very satisfactory. However, the time can vary according to how many metaphases need to be found on each slide. If the entire slide needs to be searched, the time could be much more, and it could take 30 minutes to cover all of the 2 X 4 cm tissue area. Capturing the video of the entire slide and performing the search offline at a later time, perhaps on a different computer, is another option. However, recording the video during a higher speed scan introduces motion blur that can make the metaphase recognition task much more difficult. Furthermore, the quality of the image has a large impact on the recognition success rate, and that quality depends not only on scan speed, but also on the optical and video components. So, rapid scanning is highly dependent on the hardware choices made in designing the system. The system developed in this project can scan a slide in 15 minutes with enough image quality to allow a simple metaphase finder to locate the metaphases.

Section 1.7.2 – Affordable Hardware Cost

System hardware cost is very important for most genetics labs. Budgets are limited, and the high price of medical care puts pressure on hospitals and clinics to

keep costs down. If a lab cannot justify the cost of a system by showing a significant cost savings resulting from use of the system, then they are less likely to have a budget request approved. Justifying the purchase on the basis of saving time, or faster diagnostics, may not convince the financial managers that the system is really needed. Commercially available scanning systems, with software, typically cost well over $100,000, depending on which features are purchased. One system recently purchased at OUHSC, cost $180,000. If a complete system could be sold for under $50,000, genetics labs would be far more able to purchase and use the system. Because the cost of the hardware components can be as low as $22,000, the software would have to be priced at no more than $28,000. For a system costing $180,000, the software comprises a substantial part of the final cost, even if the hardware components are at the upper end of the cost range.

In order to keep the hardware cost of this project within budget constraints, the decision was made to save money on the video portion of the system. Rather than purchase a high-end digital camera, which can cost between $15,000 and $30,000 (including frame grabber), we purchased a small analog color TV camera for under $1,000. For digitizing, we bought a $300 digital video converter which is priced for consumer use, and a two-port Firewire card costing $25 to plug into the PC. When compared with two high-end scientific grade digital cameras, the low-cost components, which take advantage of recent advances in the consumer video industry, actually outperformed the more expensive equipment. While the image quality of the digitized image is not as sharp as that visible in the microscope's

eyepieces, the video converter offers a rich suite of software-controlled features to adjust the image in real time.

The stage and its control system was priced at $15,000 (without autofocus), and this relatively high cost is worth it because of the accuracy and repeatability of the stage movements. A stage with poor performance is not likely to provide satisfactory results. We opted to purchase the joystick with the controller and its relatively low cost is well worth it because stage movement is far easier and faster with the joystick than with the usual hand turned knobs.

The microscope selected is a moderately priced laboratory grade model which provides excellent performance. Six different objective lenses can be installed in the nosepiece at one time, providing for a wide range of magnifications for scanning and still imaging. As long as only brightfield imaging with the trans illumination mode is to be used (e.g. no fluorescents or epi illumination), the modestly priced microscope is sufficient. If a laboratory already has a microscope, then an adapter is probably available to adapt the motorized stage to that microscope, allowing the lab to avoid having to buy another one.

The final hardware item for the system is a computer. There is a good deal of flexibility in this area, and most labs already own a PC that will perform the tasks required of a computer. Having a large disk drive for holding any video capture files (e.g. AVI files can be quite large if not compressed), plenty of RAM, and a fast processor are desirable features.

As mentioned, the software costs of a scanning system can easily be the most significant part of the overall investment. The man-hours required to develop a

robust and user-friendly software interface are often grossly underestimated in early budgetary estimates. In particular, the image processing portion of the programming is not only time consuming from a coding standpoint, but also requires advanced knowledge of the specialized algorithms used in this field. This difficulty makes it necessary for coding experts to work closely with imaging experts to create an effective realization of the capabilities of chromosome segmentation, identification, and labeling techniques. Processing features which do not add significant value to the system should be made optional so that the user can direct the investment funds to more useful purposes.

In summary, the hardware aspect of the system cost can be controlled by choosing good quality components, but not spending excessively on special cameras or microscopes. The hardware purchased for this project, including the microscope, were purchased for approximately $22,000. Software costs are much harder to control, and increase as more imaging features are added to the system. Only features that have a high degree of effectiveness are worth the added costs.

Section 1.7.3 – Video Image Quality

Video image quality determines the ease with which a human technician or a software algorithm can identify a metaphase spread or a pair of chromosomes. Therefore, it will also impact the speed with which a slide can be scanned and the throughput of the system. The video quality is determined by multiple factors, such as the quality of the microscope optics, the resolution and noise in the camera, and the SNR in the digital video converter. In this project, we measure the image quality by

means of the system's Modulation Transfer Function (MTF). As is described in other parts of this dissertation, selection of the video components should provide for the best image quality within the budgetary constraints placed upon the project. Selecting the most expensive components isn't necessary; it is more important that the components be carefully selected for the specific purpose of imaging metaphases and chromosomes and that the components be suitably matched for working together as a system.

Human factors are important as well, such as the adjustment of the microscope controls and the preparation of the slide. Consistent image quality makes the identification and diagnosis of the chromosomes easier, especially when software algorithms are adjusted for expected image characteristics, such as average optical density, contrast, etc. Every attempt should be made by the technician to prepare the slides and adjust the equipment the same way each time.

Based on the need to locate metaphases with a 10X objective lens, and considering that the metaphases average 50 μm in diameter, a suitable goal for the video system limit of resolution for a still image with a 10X objective is 200 lpm/mm. The system assembled in this project is capable of 225 lp/mm, as described in Chapter 2, meeting the resolution goal.

Section 1.7.4 – Accurate evaluation of metaphases

One of the best uses of a scanning system is for the system to search for, find, and evaluate the metaphase spreads, then present them to the clinical staff for evaluation. Not every cell deposited on the slide will be in the metaphase stage, and

not every metaphase cell will offer a useful spread of the chromosomes. Chromosomes which are too close together may be overlapping to such an extent that they can't be used. If they are too spread out, they may be torn or otherwise misshapen. Sometimes cell debris may be mistakenly identified as a metaphase by a searching algorithm.

If a metaphase finding algorithm presents a selection of metaphases wherein a high percentage of them are unusable, the system has probably wasted the lab's time. The technician in fact may spend more time looking at worthless cells than he or she would have spent had the searching been done manually. A tradeoff may be necessary between automated scan/searching time versus human evaluation time. In other words, if the searching time takes longer, but produces more true-positive metaphases with better characteristics, the technician will spend less time evaluating, and can devote more time to other lab duties. Scanning time will have to be increased in order to increase the accuracy of the metaphase finding, both to improve the success of the metaphase finder, as well as to select the best metaphases by means of a ranking algorithm. However, if the scan is slowed down too much, the problem again becomes on of a system that is too slow to improve the lab's throughput.

In discussing the tradeoffs with the genetics lab at OUHSC, a minimum of 80% of the metaphases presented to the operator should be analyzable, that is, suitable for karyotyping. This value was chosen for a target level that would minimize the technician's intervention, while still allowing for fast scanning. Because the metaphase evaluation feature will be part of the second phase of the system development, its measurement is deferred until that time.

Section 1.7.5 - Accurate karyotyping of chromosomes

The first four characteristics pertain to a system that is primarily designed to find and image metaphase spreads. Such a system would be useful in its own right, but does not approach the automated, or even semi-automated, diagnostic system that a cytogentics lab really needs. In order to provide for a truly advanced capability, the system needs to be able to perform the karyotyping function, or at least a significant portion of it. As described in Section 1.6, a great deal of research has been devoted to this process over the last 40 years. It is an extremely challenging task, not one that easily yields to simple methods. Karyotyping algorithms have claimed an accuracy of 80-90%, but these numbers have usually been observed only with training sets of data, not in actual clinical use. Some chromosome pairs are similar in shape and size to other pairs, and can vary in size and optical density from one cell to another. Compounding the problem is the fact that the abnormal chromosomes, those that are the object of the searching, can differ completely from the training sets that the algorithms were trained on, and the result is a substantial decrease in accuracy.

Karyotyping algorithms are being developed in our research lab, and the goal for this research is for a karyotyping accuracy of 90% for actual clinical samples. The difficulties of this challenge are significant, but the benefits make the work important enough to continue the research until a truly automated system is realized. Because this feature is also part of the second phase of the system development, its measurement is deferred until that time.

Section 1.7.6 - Minimal lab space requirements

In the typical busy clinical lab, the available space on a floor or bench is at a premium. A scanning system which includes large bulky equipment with a large footprint will be difficult to fit into the lab. Therefore, the fewer the number of components, and the smaller those components, the better it will work for the typical lab. Smaller simple microscopes, particularly ones that the lab already owns and has set up, are preferred over a large bulky type that must be moved into the lab. A small camera mounted with a C-tube mount, along with a small frame-grabber or digital converter is needed. Likewise, the controller for the stage should be as small as possible, preferably one mounted inside the computer. Autoloading, multi-slide stages can help to improve throughput but will add to the space requirements, and so must be considered from that aspect before being purchased.

If a lab has plenty of extra space, this characteristic of the system may not be that important. However, the system should be designed with the assumption that space will be at a premium. An acceptable amount of table or bench space was determined to be less than 15 square feet, including the computer and monitor. Our system can be easily arranged to occupy no more than 14 square feet or less, particularly if the stage controller and video converter are located behind the microscope.

Section 1.7.7 - Minimal operator intervention

In the ideal scanning system, an operator would set up the microscope, load one or more slide into a stage, set the system software to start a scan, and walk away.

No further interaction would be required until the cells were all karyotyped. At that point, the diagnosis could be made by the cytogeneticist. At this time, interaction is required with any of the systems that are available commercially. Most of the interaction occurs when the technician must look through the metaphases that have been located by the searching algorithms, and again when the karyotyping software has tried to identify the chromosomes. If the microscope stage can only work with one slide at a time, then the operator will spend significant amounts of time positioning and removing each of the slides between scans. Likewise a metaphase finder that presents a large number of false-positives, or a karyotyper that is prone to a high rate of errors, will require even more intervention. If so much intervention is required that the lab workers are tied down to interacting with the system for the majority of the time that it is being operated, then the system is offering very little value to the lab. Manual methods would be nearly as fast.

In order to reduce operator intervention, automatic slide loaders and multi-slide stages are important. (Their monetary cost must be carefully considered, however). At the same time, the accuracy of the software algorithms has a significant effect on the amount of intervention required. As a target goal for the time required, there should be no more than five minutes of intervention needed for each karyotype obtained. This time would not include loading/unloading the slides, but all other user actions would be counted. This measurement is also deferred until Phase II.

Section 1.7.8 - Installed on lab's own computer and microscope

A system which can be installed on equipment that the lab already owns is one way of saving both money and lab space. Most of the motorized stages available can be adapted to a large number of the most popular lab microscopes. Therefore, a system which can work with a typical commercially available lab microscope will probably be more affordable to the typical lab. In the same way, most labs already have computers with most of the features that would be needed to control the stage, receive the video stream, and process the video. The addition of a Firewire port card may be required, or perhaps some added memory, but these components are readily available at minimal cost. If a computer and microscope that are already situated on a lab bench can be used, then the amount of extra space that the system will require is minimized.

Both cost and space can be reduced if the system is constructed from standard off-the-shelf components. This goal was easily met by specifying a stage that can be adapted to the most common models of laboratory microscope and computer software that is PC Windows based.

Section 1.7.9 - Minimal training requirements

To be cost effective, a scanning system should be designed to be operated by lab personnel who have only modest computer and biomedical skills. While a cytogeneticist with an advanced education and years of experience is necessary for approving a karyotype and providing a diagnosis, a lab technician with a much lower level of knowledge should be able to use most of the features of the system.

Advanced computer skills or indepth knowledge of image processing algorithms are not likely to exist among the typical clinical worker. Complicated operations or lengthy training sessions are common sources of frustration with many types of automated systems and frequently lead to poor results and user dissatisfaction. Because the software will run with a Windows GUI, the typical lab worker will have little trouble learning the most important system functions. The training program and its evaluation are deferred until Phase II.

Section 1.7.10 - Flexible selection of imaging options

This system characteristic includes image filtering and enhancement tools. Such tools are standard in image processing software, such as Adobe Photoshop. If used properly, they can improve the appearance of metaphase and chromosome features, perhaps increasing the performance of the recognition algorithms by correcting for variations in illumination levels and contrast. However, if use of these tools requires significant training to by used effectively, as mentioned in the previous section, then it would probably be better to direct the programming resources to other system capabilities and simply adjust the video filtering for average conditions.

The imaging options will be software functions that will be implemented in Phase II.

Chapter II – Hardware Components of a Microscope Scanning System

Section 2.1 – Introduction

Careful planning is necessary to develop a hardware system that meets meaningful specifications while fitting within budgetary limitations. Table 2.1 shows specifications set out for hardware performance and their measurement in the implementation of the system plan. Some of them overlap with the system goals discussed in Chapter 1, but here they will be discussed as specific hardware performance requirements. These specifications were determined early on in the project

Specification	Goal	Achieved	Goal Met Y/N ?
Stage Speed	> 10mm/sec	100mm/sec	Y
Stage Accuracy	Less than ±10 µm	±3 µm	Y
Video Resolution	200 lp/mm at 10X	225 lp/mm	Y
Magnification	10X, 60X, 100X	10X,20X,40X,100X	Y
Camera Frame Rate	30 fps	30 fps	Y
Computer CPU Rate	> 1 GHz	2 GHz	Y
Computer Ram	> 1 GB	2 GB	Y
Computer Disk Size	> 100 GB	120 GB	Y

Table 2.1 – Hardware Performance Goals

by studying the basic problem at hand and by examining the hardware in use at the OUHSC. Each of these specifications will be discussed in the sections to follow.

Fig 2.1 shows a block diagram of a basic microscope scanning system. Fig 2.2 is a photograph of the system components. The heart of the system is a high-quality laboratory grade microscope, available from manufacturers such as Nikon and Olympus.

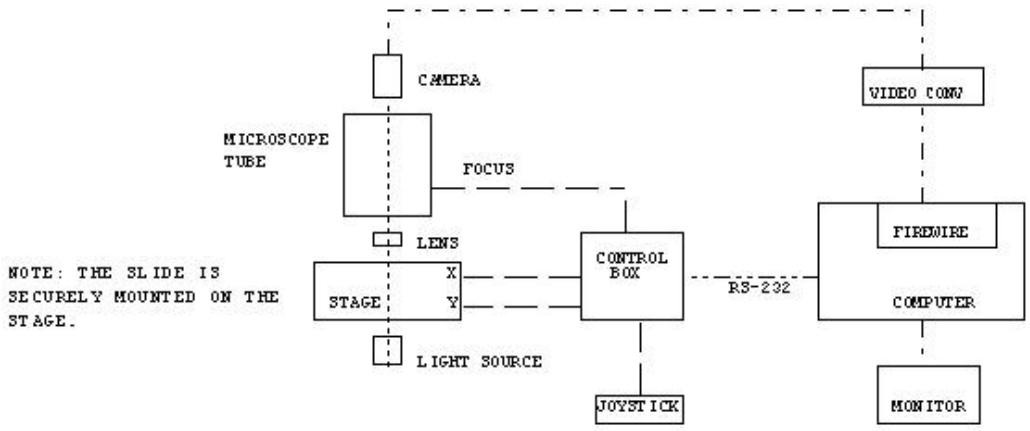


Fig 2.1 – Diagram of Microscope Scanning System

The microscope will usually accept up to six different objective lenses. Objective magnifying powers from 10X to 100X are readily available. The lower power lenses are usually of the "dry" type, meaning that mineral oil is not required for their use.

Higher magnification lenses are frequently of the "oil" type. For these lenses to work properly, a drop of mineral oil, having a specific index of refraction, must be used between the lens and the slide (or coverslip). Without the oil, the magnifying

power and resolution of the lens are greatly reduced. An oil lens would not be suitable for scanning. The oil would dry out while the scan was in progress, making the image quality very inconsistent. A 100X oil lens is most likely to be used in a still image mode, when the chromosomes are being imaged for charyotyping. Matching coverslips should be available for use with lenses that are designed for coverslip use. Without the coverslip, the resolution would be affected. However, lenses that do not require coverslips are more convenient for scanning

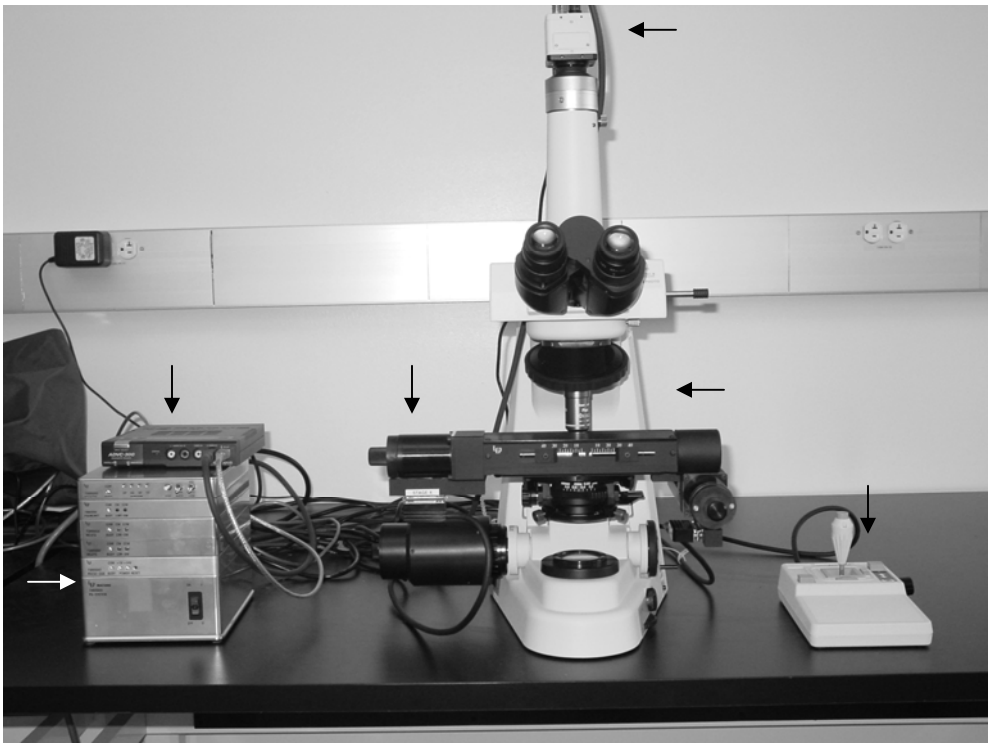


Fig 2.2 – Photo of Microscope Scanning System

chromosomes, where the nature of the stained material makes coverslips unnecessary. Standard coverslips do not cover all of the area that needs to be scanned. Larger

coverslips are available, but would be more subject to vibration during scanning, possibly distorting the image.

The microscope should have a continuously adjustable light source, allowing a light level that is optimized for ambient light conditions and also for the particular video system in use. It should be possible to install one or more light filters in the path of the light source in order to optimize the visibility of the metaphases and individual chromosomes. The light path aperture should be adjustable in order to adjust the image for optimized contrast or maximum resolution, depending on the task at hand. The vertical position and the aperture of the condenser should be adjustable in order to obtain the best compromise between resolution and contrast.

The stage is the part of the microscope which holds the specimen slide. In order to easily view the entire slide in a controlled manner, the stage should have controls for the position of each axis, in this case X and Y axes. In this application, it is very important that the axis controls be precise and stable. There should be no backlash or drift in the controls. Once the stage is moved to a particular position under the objective lens, heat and vibration should not cause any significant drift in the position. A spring loaded device should hold the slide down firmly so that it does not move or vibrate during a scan.

For automated scanning, the stage must have motors to move the stage independently in the X and Y directions. These movements must be extremely precise and accurate. Control circuitry is necessary to receive commands from the computer and to translate the commands into voltage to drive the motors at exactly the right speed and for the right length of time in order for the slide to be properly

positioned. For this system, the stage is controlled by a control box matched to the stage by the stage manufacturer. A joystick connects to the control box and allows for variable speed movements and other helpful control features.

Some means of focusing the objective lens must be provided, both for course focus and for fine focus. The microscope is equipped with an autofocus motor, also called a Z-axis motor, mounted on the lower left side of the microscope base. The autofocus should still allow the user to operate the focus manually. Autofocus capability can be extremely useful when the objects to be imaged vary in their thickness or vertical position. The autofocus control circuitry can be integrated with the stage motor controls. In the case of searching for metaphases under 10X power, the focus is fairly uniform throughout the slide.

A scientific grade video camera is mounted on the microscope's C-mount tube in order to capture the images to a digital file. For metaphase imaging, either a color camera or B/W camera are sufficient. High resolution and adjustable sensitivity are essential in order to clearly view the metaphases. The camera should either be a digital camera, or be interfaced with a digital video converter. The converter can be either a *frame grabber* card installed in a computer, or an external stand-alone converter. If an external converter is used, the computer will require some sort of communication port to receive the digital video data. The USB2 serial bus or Firewire® (IEEE 1494) serial bus are commonly used for this purpose. Data transfer rates of 40 MHz or more are necessary when capturing live video, and either of these two interfaces are satisfactory. For this project, a commercially available digital video converter was purchased. These converters are available in a wide range of

prices and features. The Firewire serial cable is used to interface the converter to the PC. The PC has a Firewire card installed in one of its card slots.

The computer should be equipped with a large disk drive, at least 100 GB, DRAM of at least 1 GB, and a processor speed of at least 1 GHz. A large monitor is desirable, 17" or better. A control port, either RS-232 or USB, is necessary to communicate with the stage controller. Software must be installed in order to communicate with the stage controller and to capture and process the digital video.

Section 2.2 - Motorized Stage Design

Modern motor designs and control techniques, together with the wide availability of numerically controlled milling machines, have made it possible to manufacture microscope stages with outstanding accuracy and resolution. Controllability, repeatability, and accuracy of a few microns is now common for moderately priced stages. Control increments of tenths of microns is especially convenient for automatic scanning and locating features on microscope slides. Using stepper motors with micro-stepping control techniques, digital position encoders, DSP-based microcontrollers, and carefully milled mechanical drives, the new designs make it possible to locate XY coordinates with excellent repeatability.

The heart of the mechanical design of a good stage is a solid base which maintains its coplanarity and alignment under all conditions of temperature and humidity. Usually made from anodized aluminum, the base must provide a stable and level platform upon which to mount the slide.

An adapter ring allows the stage to be securely mounted to whichever microscope the lab is using. State-of-the-art CNC machines can mill the base directly from a CAD design file with extremely good accuracy. Mounting holes must be drilled with errors of much less than 0.1 micron if the stage is to move with acceptable accuracy. Precision ground crossed roller bearing guideways minimize translational errors and allow for smooth travel without vibration. Recirculating ball leadscrews transform the motor's rotational motion into highly precise linear movements. Limit switches along each axis allow the stage control box to determine reference points for its coordinate system. The components of the stage must be relatively insensitive to temperature changes in order to avoid misalignment errors.

While a variety of motor types and designs could be used for designing a high precision stage, stepper (or stepping) motors are often the most accurate and convenient to use [41,42]. The idea behind a stepper motor is that movements are in discreet steps which are determined by the mechanical positioning of the stator poles and the number of teeth on the stator and rotor. While linear stepper motors could certainly be used to move a stage, it is common to use rotating motors and provide a gear train and lead screw to transform to linear motion. This is because a gear train working with a lead screw can reduce the motor's rotational steps to extremely small linear movements.

A motor drive requires some sort of control circuitry to obtain the proper speed and displacement of the motor shaft. For a stepper motor operated in the full-step mode, the control circuitry could be as simple as a combination of flip-flops and logic gates. However, the flexibility of microcontrollers allows for many more

options, such as directional control, rotation speed, and driving mode. Furthermore, in cases where exceptionally accurate movement is needed, a digital encoder can be mounted on the motor shaft which can be read by the microcontroller as a means of closing the control loop. The feedback provided by the encoder will allow for error correction in the unlikely event of an error, and give an accurate indication of motor speed. It is possible that a stepper motor could become unstable if accelerated too quickly. If the control system is open loop, the maximum rate of acceleration has to be limited to ensure that the motor won't break into oscillations. With a closed loop system, however, any unstable motion will be detected by the microcontroller, and correction can be applied to eliminate errors. Thus, a closed-loop system offers the advantage of higher acceleration with minimum error probability.

Today, the microcontroller of choice for motor control use is the DSP-based controller. These devices have many features that make them ideal for controlling all types of motors, including steppers. Clock speeds of 40 MHZ or more allow for extremely quick reaction to changing torque or position requirements. A full complement of I/O pins allow polyphase motors to be controlled easily. DSP chips with DAC capability allow for driving stepper motors in the microstepping mode, with a wide choice of transistors to interface the chip to the motor windings. The digitally encoded representations of the voltages corresponding to sinusoidal microstepping waveforms can be stored in a lookup table in the device's internal memory for sequential output to the DAC pins. The DAC output pins can then drive the transistors which provide drive current directly to the motor windings. Built in multichannel A/D converters, combined with small series resistors, can serve to

monitor motor phase currents. For cases where the driving waveforms are extremely complicated, a rich suite of built-in math functions allow for output drive levels to be accurately computed on the fly, rather than drawn from a look-up table.

With a digital encoder providing speed and position feedback, and the phase currents reflecting the load requirements, the microcontroller can adjust the driving waveforms to closely control the torque and/or speed of the rotor, or shut down the motor in case of a stall condition. Also, DSP based controllers are convenient for power factor correction in inductive systems, a feature which is mandatory in some countries. DSP algorithms, using the built-in registers, allow for digital filtering algorithms to be used on any feedback signals that might have noise signals impressed on them. Communication ports let the DSP controller communicate with a large variety of other devices, such as in the ethernet linked systems, USB, or older RS-232 or RS-422 devices.

Most motor control systems today have the capability to interface with a computer of some sort for external control or monitoring. In the past, the interface was likely to be an RS-232, RS-488, or RS-422 link. Today, USB or Firewire ports are likely to be included with a motor control box. However, in an industrial environment, it is now common to have a motor controller communicating with a factory-wide control system via an ethernet cable or WIFI hookup. For a microscope stage, especially where a video camera and digital video converter are used to capture a slide image, a USB 2.x or Firewire serial hookup is appropriate. The high data transfer rate of these channels, along with the ability to daisy-chain devices, is ideal for this application. The controller should be able to communicate with the computer

with simple ASCII based commands that allow for complete control and monitoring of the motor movements and stage position. It should be possible to use a variety of software languages, such as C/C#/C++ or Visual Basic, to write the code which the user's application program needs to control the stage.

Section 2.3 – Video Camera

A good imaging system is essential if the high-quality images produced by the optics of a good microscope are to serve a useful purpose when digitized. A poor camera system can degrade the image enough to cause ineffective diagnoses and frustration for the microscopist. This section will explore some of the important aspects of cameras used in light microscopy. Cameras can be extremely expensive and it is important to purchase a camera that is sufficient to perform the imaging tasks without wasting funds on a camera that has features that are not important. As of this writing, it is easy to spend more on a camera than on a microscope, but it is important to divide the expenditures so that the two instruments compliment each other.

In this project, colored video is not necessary and may even be considered inconvenient, since ultimately the image will have to be converted to grayscale in order to do image processing. However, color video cameras with excellent performance are reasonably priced due to mass production, so buying a color camera may in fact be the best choice. The conversion to grayscale may be done in a video converter or in software.

As previously mentioned, the camera must be provided with a lens (an eyepiece) which properly focuses the real intermediate image at the objective's back

image plane onto the camera's detector. The lens and camera are meant to be mounted on the microscope through an interconnecting tube known as a *C-mount* tube. The lens, sometimes referred to as a *relay* lens, will require a tube that positions the lens entrance pupil at the back image plane of the objective. The magnified image will then be focused onto a frame of film in a film-type camera, or onto an electronic detector in a digital or video camera. The electronic detector may be connected to digitizing circuitry which will output the pixel values in digital format, or the detector's output may be made available as an RGB, or YUV, or S-Video analog signal.

The two most important design characteristics of the camera used in microscopy are the pixel pitch, which affects the resolution of the system, and the detector noise [36,37]. Maximum frame rate, detector size, dynamic range, and cost are also to be considered, but the pixel pitch and noise are essential if the overall system is to provide high quality images. The pixel pitch is defined as the distance between the midpoints of adjacent pixels. Fig 2.3 shows a simple diagram of a possible layout of a digital *charge-coupled device* (CCD) detector, a digital type of video detector. The detector is constructed in a square, with picture elements, or *pixels*, representing the individual active detecting points. The number of pixels in the horizontal dimension is the same as the number in the vertical dimension. The pixel size in this simple example is 12 μm by 12 μm, with 1024 pixels in the horizontal dimension, and the same number in the vertical dimension.

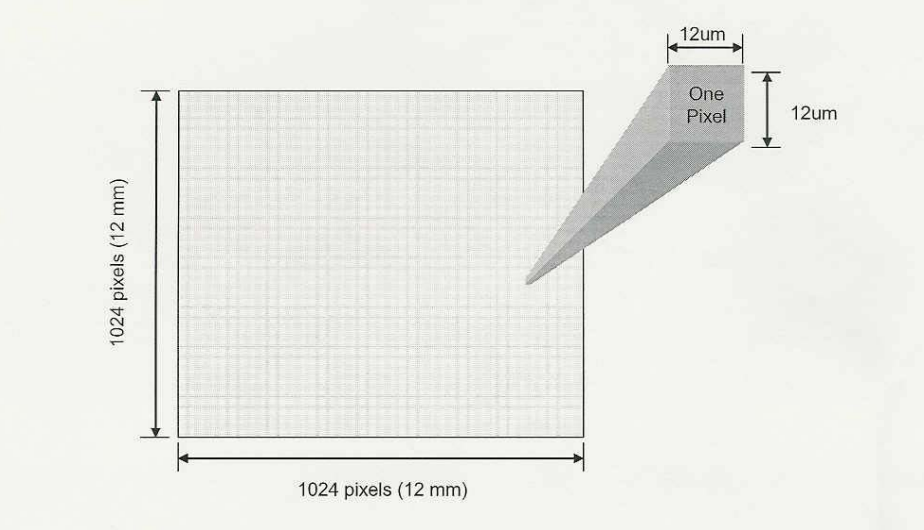


Fig 2.3 – A camera CCD detector layout.

The total size of the detector chip would then be

$$1024 \times 12\ \mu m \approx 12\ mm \qquad (2.1)$$

on each side. Each pixel presents an active silicon detector that produces charge proportional to the number of photons striking the pixel during each sample period. Figure 2.4 show a drawing of a semiconductor light sensitive pixel element.

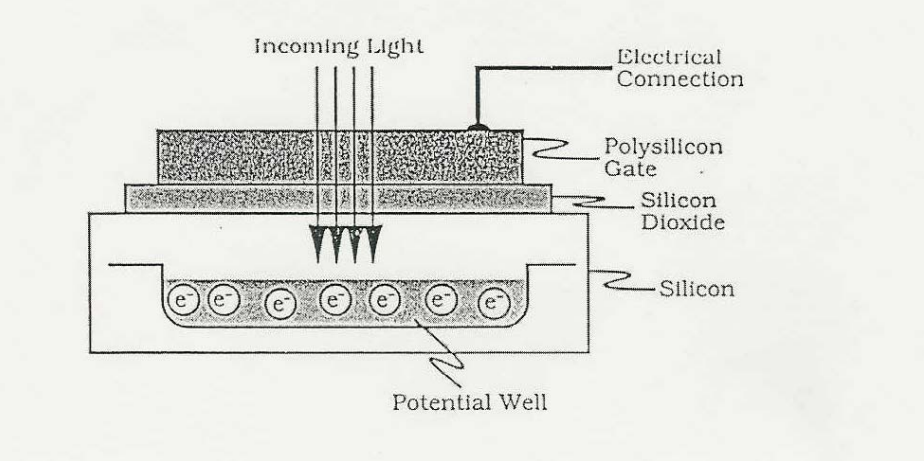


Figure 2.4 – Semiconductor CCD pixel detector

The detector is fabricated from a silicon substrate, a silicon dioxide insulator, and a polysilicon gate. A bond wire forms an electrical connection to the gate, which allows the device to be controlled. The substrate forms the other electrode, making the device a solid-state capacitor. The capacitive charges are held in the substrate in a structure called the *potential well*. When light photons impact the device, doping atoms in the n-type substrate are ionized, producing charge carriers. The resulting free charges are proportional to the number of photons received. During a clocked sample period, the charges accumulate. At the end of the period, the charges are transferred, or coupled, to a register which interfaces each row and column of pixels to analog-to-digital converters (ADC). The outputs of the ADCs form the digitized image.

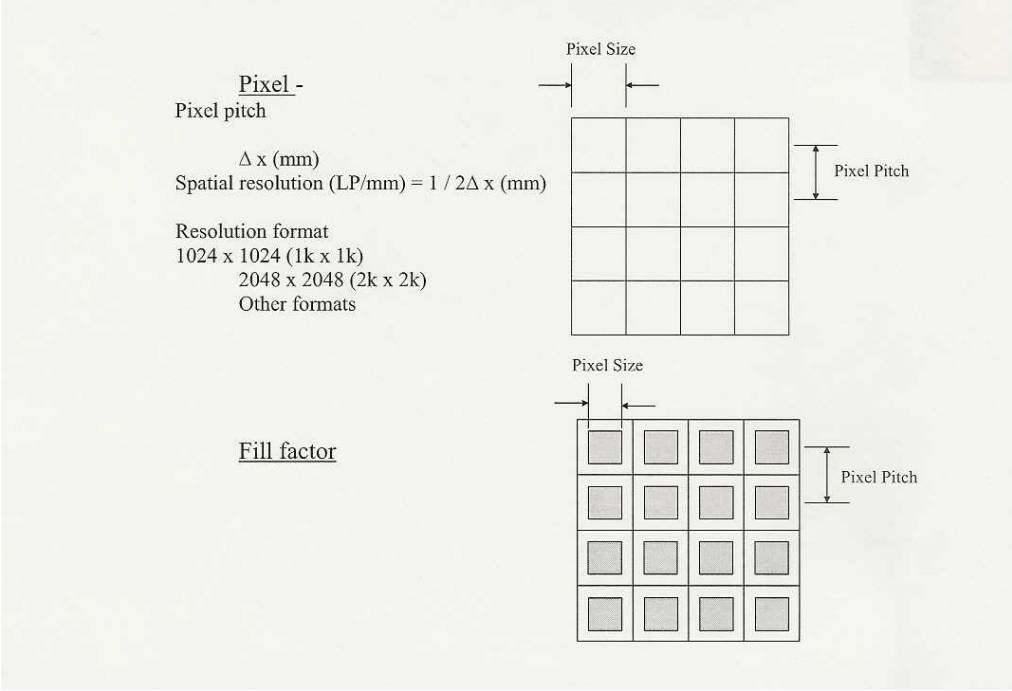


Figure 2.5 – Relationship between pixel size and pixel pitch. Fill factor affects pixel size, but not pixel pitch.

The amount of charge read from each pixel then forms the electrical signal that is used to represent the light intensity detected during that sample period. After the charges are transferred out of the pixel potential well, the well is cleared of charges and is ready for the next exposure sequence.

The separation between the pixels, or pixel pitch, is shown in Fig. 2.5 as Δx. The best (unmagnified) resolution of this device is therefore found by the following formula:

$$d = \frac{1}{2\Delta x} \text{ lp/mm} \qquad (2.2)$$

where *d* represents the limit of resolution, or the minimum separation between objects that can be resolved, and ΔX is the pixel pitch. The units of *d* in this case are line-pairs per millimeter (lp/mm). The name refers to the fact that etched gratings are often used to measure resolution in imaging, and they are etched with closely spaced lines with the spacing measured as the number of bright/dark transitions, or line pairs, within the distance of 1 mm.

Fig 2.5 also shows the relationship between pixel size, pixel pitch, and *fill factor*. The fill factor refers to the percentage of the pixel area that contains active photosensitive material. Some of the CCD chip's area must be reserved for the support of the active devices, as well as for connecting paths for the transfer of charges, so the fill factor will be something less than 100%. A low fill factor will imply that the active device will receive fewer photons during a sample period, and so will be less sensitive to light from weak sources. As seen in the figure, the fill factor affects the pixel size, but not the pixel separation. For scientific-grade CCD detector chips, the fill factor will be very high, sometimes nearly 100%.

Section 2.4 – Scanning Methods

There are two main ways to perform a scan. One method is to move the stage in small increments, capturing a single frame while the stage is stationary, then moving the stage again for the next frame. In this way, the entire slide is captured as a series of still images. In some applications, the still images are "stitched" together to make a continuous video image of the entire slide. This method has the advantage of eliminating motion blur from the image, and is the preferred method if the purpose

of the scan is to produce a high quality continuous video image for detailed examination. The other method is to scan the slide in a continuous motion, with real-time video. The advantage of this method is the increased speed, since the stage does not have to start and stop thousands of times during the scan. Reduced wear and tear on the stage motors is another advantage. The disadvantage of this method is obviously the motion blur that degrades the image. However, in the case of a system scanning for metaphases under low magnification, the main purpose is to find the location of the metaphases. If the metaphases can be found in the captured video, by human or software, in spite of some motion blur, then the improved scan speed makes this method highly desirable. In the case of the metaphase finding scanning system, the end goal is to find the metaphases quickly so that they can then be viewed as a still image under high magnification. Thus, the motion blur is not a problem as long as the metaphases can still be found.

It is not necessary for the stage to scan the entire slide. Only part of the slide will contain tissue that needs to be searched. Figure 2.6 shows a diagram of the slide, showing the part that needs to be searched. The search area covers a 4cm X 2cm portion of the right hand part of the slide. In order to reduce the total scan time, it is logical to scan the slide in a horizontal motion, the horizontal dimension being the longest. In this way, half of the trips across the slide will be left to right, and half will be right to left. This reversal of direction will have to be accounted for in the metaphase searching and finding algorithms. After the edge of the slide is reached, the Y-axis motor will move the stage in the Y direction in order to position the slide

for the next horizontal trip. The size of the Y-axis movement will be referred to as ΔY.

Figure 2.7 helps to determine the size of the field of view when using the 10X objective. An image of the stage micrometer was obtained by converting a frame of video to a JPEG file. A small section of the 100 µm scale was extracted from the image.

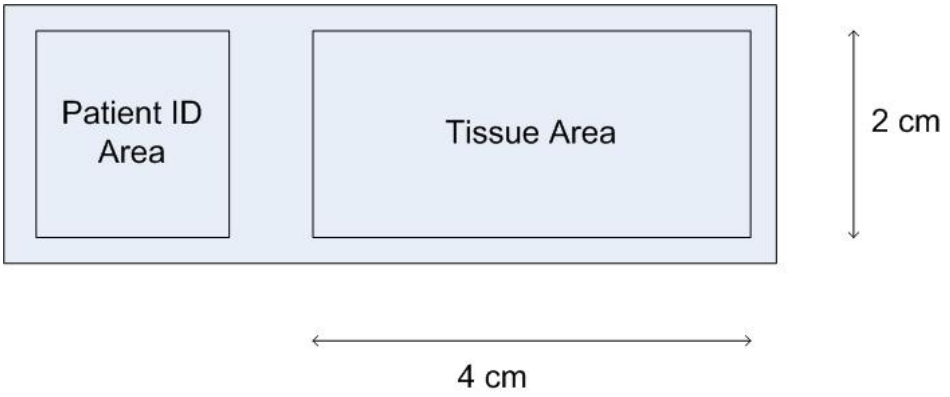


Figure 2.6 – Diagram of slide areas.

The pixel values of that section are shown in the figure. The numbers in bold are pixel values which correspond to the black areas of the scale. These numbers are relatively small, but not zero, showing that they are not perfectly reproduced by the camera. The larger numbers represent the bright areas around the scale, where the light is coming through unimpeded. The bold numbers on the far left represent the vertical scale line at the 20 µm point. The bold numbers on the far right represent the vertical line at the 40 µm point. The dark cluster of numbers in the center correspond to the smaller 30 µm mark. In between these regions are the smeared 2 µm marks.

244	**113**	**135**	248	255	240	255	253	245	250	253	255	217	167	193	239
245	**92**	**138**	245	255	242	225	255	251	253	246	255	228	**74**	184	239
255	**65**	**132**	253	249	255	229	160	184	226	255	255	192	**63**	167	244
188	**27**	**80**	172	172	185	**138**	**60**	**121**	166	197	194	**136**	**69**	**135**	198
105	**17**	**33**	**76**	**103**	**85**	**27**	**46**	**70**	**74**	**72**	**75**	**63**	**62**	**73**	**88**
132	**31**	**49**	**110**	**137**	**106**	**53**	**91**	**107**	**106**	**98**	**102**	**102**	**107**	**106**	**103**
222	**38**	**96**	216	217	207	170	**129**	**130**	166	183	179	**147**	**100**	**142**	163
255	**70**	**137**	255	249	255	237	184	201	244	255	249	209	**113**	203	240
253	**126**	169	241	244	247	238	255	248	255	240	237	223	**109**	222	249
247	156	179	251	255	237	255	248	255	251	255	250	211	177	203	255
255	203	220	255	255	245	255	245	255	251	255	255	239	221	232	255

Figure 2.7 – Pixel values for 20 μm segment of stage micrometer.

They are quite clear and distinguishable in the 10X eyepiece, but not in the camera image. This difference is a manifestation of the limited resolution of the camera reducing the overall system resolution.

By counting the number of columns between the two tall lines, we find that a 20 μm distance is separated by 12 columns of pixels. Therefore, each pixel horizontally represents approximately 20μm /12 pixels = 1.7 μm /pixel. Since the overall dimensions of the JPEG image is 640 x 480 pixels, the horizontal field of view is:

$$640 \text{ pixels} \times 1.7 \text{ μm /pixel} = 1067 \text{ μm}. \qquad (2.3)$$

In order to measure the vertical field of view, we rotate the camera 90 degrees and repeat the experiment. In this way, the vertical pixel size is also found to be 1.7 μm /pixel, giving a vertical field of view of

$$480 \text{ pixels} \times 1.7 \text{ μm /pixel} = 816 \text{ μm}. \qquad (2.4)$$

Using the same method, the pixel sizes for the 20X, 40X, and 60X lenses are found to be 0.83 μm /pixel, 0.4 μm /pixel, and 0.27 μm /pixel, respectively. These values are consistent with the fact that the image is being magnified.

Now we need to determine the diameter size of a typical metaphase grouping. We can do this several ways. Figure 2.8 shows an image with an arrow pointing to a metaphase, and superimposed with the micrometer scale for comparison. As can be seen, the metaphase is slightly less than three major divisions across, with each division at 20 μm separation. Examination of dozens of metaphases shows that most are between 40 μm and 60 μm, and are approximately circular in shape.

Since the larger metaphases are approximately 60 μm in diameter, we can calculate the value of ΔY that will allow the tissue area to be scanned with as few trips as possible while still ensuring that every metaphase will be captured in the

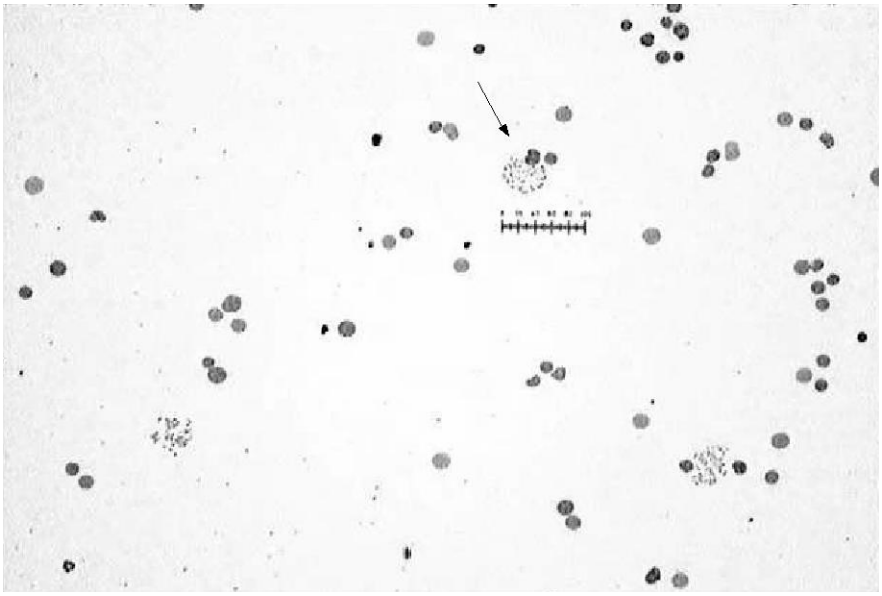


Figure 2.8 – Metaphase with micrometer scale superimposed.
Diameter of metaphase is slightly less than 60 μm.

images. With the 10X objective lens selected, the vertical field of view for the camera is approximately 800 μm. We could simply conclude, then, that the correct value for ΔY would be 800 um. However, some metaphases could then be cut in half and missed. Therefore, we should allow for some overlap of the field of view and reduce ΔY to 800 – 60/2 = 770 μm, in order to have a better chance of capturing all, or at least most, of each metaphase image. So, in order to cover a 2 cm vertical range, we will need in order to

$$\frac{2cm}{770um} = 26 \text{ horizontal trips} \qquad (2.5)$$

completely cover the tissue area. The amount of time it takes to scan the tissue area is therefore dependent upon the size of the vertical field of view as well as the motor speed. It is easy to see that scanning with a higher power lens, say 60X, with its much smaller field of view would require a much bigger number of horizontal trips, thus increasing the required scan time accordingly.

It is desirable that scanning a single slide should take no more than 15 minutes. In order to meet that goal, we need to calculate how fast the X axis will have to move. The total horizontal distance to cover is given by:

$$4 \text{ cm x } 26 \text{ trips} = 104 \text{ cm} = 1040 \text{ mm.} \qquad (2.6)$$

The vertical movements will add a small amount of time to the total scan, but since we can move the vertical axis at high speed without blurring the image

excessively, the horizontal time will be far more important. So the horizontal scan speed will have to be

$$\frac{1040mm}{15\,\mathrm{min}} \times \frac{1\,\mathrm{min}}{60\,\mathrm{sec}} = 1.16mm/\mathrm{sec} \qquad (2.7)$$

in order to cover the 4 cm horizontal width of the tissue area. The important question is: if the stage is scanned at that speed, will the image be blurred so badly that the lab technician cannot recognize the metaphases on video playback, or that a pattern recognition algorithm cannot find them? This question will have to be answered by experimentation.

Section 2.5 – Determination of Microscope Resolution

Next to the value of *M*, the magnifying power, the next most important characteristic of an objective is what is known as the *numerical aperture*, *NA* [36,37,40]. The numerical aperture is a measure of the angular opening of the lens. In other branches of optics, cameras for example, the so-called f-number (f/#) is a convenient way of rating lens performance. But, for microscopy, numerical aperture is more meaningful. It is calculated by the following formula

$$NA = n\sin\theta \qquad (2.8)$$

where n is the refractive index of the medium between the lens and the sample, and θ is the half angle of the cone of diffracted light entering the lens. For the dry lens that

we are using in this project for scanning, the intervening medium is air, so n = 1 and $NA = \sin\theta$.

The diffraction pattern also depends on the wavelengths present in the illuminating light wave. The following formula expresses an important relationship

$$d = 1.22\lambda / 2NA \qquad (2.9)$$

where d is the radius of the diffraction spot produced by a point source, λ is the wavelength of the illumination, and NA is the numerical aperture. This relationship shows that the minimum distinguishable size of small details in the chromosomes increases with increasing wavelength and decreases with increasing numerical aperture value. The value of d also determines the ability of a lens to separate two or more closely spaced objects. If the objects are separated by a distance less than d, they will appear to touch or overlap in the image. Two objects which are smaller than d, but separated by more than d, will not touch or overlap in the image, but their size will be nevertheless distorted, each appearing to have a radius of d.

As an example, suppose that the Nikon 10X Plan objective lens, with an NA value of 0.25 is used to image a metaphase. Further assume that a halogen light source is used which has strong spectral content around 600 nm. The resulting diffraction spot diameter would then be:

$$d = 1.22 \cdot 600 / (2 \cdot 0.25) = 1464 \text{ nm} = 1.46 \text{ μm} \qquad (2.10)$$

Therefore, the smallest metaphase feature that could be imaged at its proper size would have a radius of 1.46 μm. Since a typical metaphase has a radius of approximately 20 μm, with important textural details of approximately 5 μm, this spot size is quite acceptable for the task of metaphase finding. However, the spot size seen in a digitized version of the image will probably be larger, due to the degrading effects of the camera and digitizer. When a microscope has an actual spot size agreeing with the above formula, the instrument is said to be *diffraction limited*. This expression implies that lens aberrations (such as spherical and chromatic aberration) have been corrected sufficiently to make the diffraction equation the limiting factor in the value of *d*.

Generally, but depending on the lens design, the higher the magnifying power of an objective lens, the higher the value of *NA* and so the better the resolution. Therefore, when imaging the chromosomes with higher power, the size of the diffraction spot is reduced. When using the 60x lens with *NA* = 0.8, the value of *d* drops to 572 nm, 0.57 μm. It must also be kept in mind that the condenser *NA* must be greater than or equal to the objective *NA* , and for the condenser aperture and all other adjustments properly made, for these *d* values to be meaningful.

The 20X and 40X lenses purchased for this project both have NA values of 0.75, three times larger than the NA of the 10X lens, and just slightly less than the 0.8 for the 60X lens. The 100X oil lens has an NA value of 1.25.

Since a higher value of NA gives better resolution, it might seem that selection of a lens should always put maximum importance on NA. However, there is another factor affected by the value of NA. The d*epth of field* (DOF) is a measure of

how much of the depth of the specimen is in focus at the same time. This value is given by

$$Z = n\lambda / NA^2 \qquad (2.11)$$

where Z is the depth of field, n is the refractive index of the interface, λ is the illuminating wavelength, and NA is the numerical aperture. For our 10x lens, with an air medium, this corresponds to a depth of field of

$$Z = 1 \cdot 750 / 0.25^2 = 12\ \mu\text{m} \qquad (2.12)$$

From the formula it can be readily seen that if the NA is made larger, the value of Z is decreased. However, in the case of imaging metaphases, which are contained in a thin layer of dried solution on a slide, the depth of field is not as important as it would be if we were examining live tissue suspended in liquid solution. Therefore, objective lenses with large NA values will not impair the quality of the focus for metaphase finding and karyotyping.

Another factor to consider when choosing an objective lens pertains to the light gathering power or image brightness B. B is defined through the relationship

$$B \propto (NA / M)^2 \qquad (2.13)$$

where M is the magnification of the lens. The relationship also depends on other factors, such as the illumination level being used, and other lens design factors. As can be easily seen, a lens with a higher value of NA, for a given magnification, will produce a brighter image. For our 10X lens, we have

$$B \propto (0.25/10)^2 = 6.25 \text{ x } 10^{-4} \qquad (2.14)$$

while for the 60X lens, we have

$$B \propto (0.8/60)^2 = 1.78 \text{ x } 10^{-4} \qquad (2.15)$$

The fact that the 60x lens has a lower value of B explains why we find it necessary to increase the illumination setting on the source in order to obtain an equivalent brightness when switching from the 10X lens to the 60X lens. Therefore, there could be a problem for an automated system which requires a change of objective lens during a scan/recognition procedure, perhaps using an automatic lens changer. The illumination level would have to be adjusted for the lens change, and the light bulb intensity cannot usually be adjusted automatically. It can be noted that if the microscope is properly adjusted, the focus should be correct when changing lenses; this is what is meant by the term *parfocal*. But, there is no guarantee that the illumination will be correct. While illumination can be partly corrected by image processing, the image quality may still be adversely affected.

As the diffracted light travels upward from the slide, it enters the objective lens orifice. The objective lens is the primary means of magnifying the image, with magnification values of 10X to 100X in common laboratory use. The optical interface between the sample and the objective lens is important, mainly because it involves a change in refractive index of the media. Objective lenses can be designed to be used with an air interface, such as our 10X dry lens, a glass/air interface, such as our 60X lens, or a glass/oil interface, such as our 100X lens. A glass/air interface type of objective lens is intended to be used with a glass coverslip placed on the top surface of the slide. The slide is assumed to be of standard 1.1 mm thickness, and standard coverslip thickness is 0.17 mm. The refractive index of the glass is supposed to be 1.515; the same value of n is specified for the immersion oil. The thickness and refractive index of the coverslip is important because the angular extent of the diffraction pattern entering the lens aperture is greatly affected by the interface. For example, if a dry lens is used (with appropriate coverslip) any light rays subtending an angle of 41º or greater are lost by total internal reflection at the air/lens interface, and never enter the lens. For this reason, a dry lens has a practical limit of about 39º incident angle. Geometry shows that an incident angle of 39º results in a 72º half-angle of light entering the lens. Using the formula for the numerical aperture, (with $n = 1$)

$$NA = n \sin\theta = 1 \text{ x } \sin(72^\circ) = 0.95 \qquad (2.16)$$

meaning that the best dry lens is limited to a maximum *NA* of 0.95. Converting this value to resolving power, we have (at $\lambda = 600$ nm)

$$d = 1.22 \cdot 600 / (2 \cdot 0.95) = 0.39\ \mu\text{m} \qquad (2.17)$$

the limit of spatial resolution for the best dry lens. If an oil lens is used, light which might otherwise be subject to total internal reflection, and not reach the lens, is instead transmitted through the coverslip/oil interface and into the lens. Oil immersion lenses are more often used with higher power objectives (e.g. 100X) when viewing chromosomes for karyotyping purposes. In this project, scanning is done with a 10X objective lens which is designed to be used without a coverslip.

Section 2.6 – Measuring the Modulation Transfer Function

The standard way of evaluating imaging equipment is by means of the Modulation Transfer Function, or MTF [36]. It allows an objective means of comparing optical systems. A chromosome scanning system will be subject to factors that will degrade the quality of the image. Limits of resolution, focus problems, and digital noise are some examples of these factors. The degradation usually appears as a blur in the image, or a decrease in sharpness. Fine lines and small details begin to spread out and blur together. The measurement of the MTF provides a way to quantify the blur. When the features are moving, as they are during a full motion scan, the blur is made worse. The pixels of a feature will be detected by more than one pixel of the detector while a frame is being read. Pixels of the feature start

overlapping and the result is a blur. In this chapter, we consider the methods of measuring the MTF of the scanning system, with special emphasis on evaluating the motion blur.

Fig 2.9 shows an example of a target that can be used to measure lp/mm in a microscopic system, imaged with a 10X objective. The stage is stationary for this image. This target is referred to as "USAF 1951" due it being specified by the United States Air Force in 1951 for calibrating optical systems. The target is made of glass and is etched so that the lines and numbers are transparent, allowing light in the *trans* mode to shine through. Other areas are painted black, allowing no light to penetrate to the microscope's objective lens. A chart that comes with the target gives the number of lp/mm, actually expressed as cylcles/mm, for each of the elements and groups in the target. For example, Group #7 is in the center of the picture. Underneath the '7' there are six groups of horizontal and vertical lines. The lines directly beneath the '7' compose element #1,

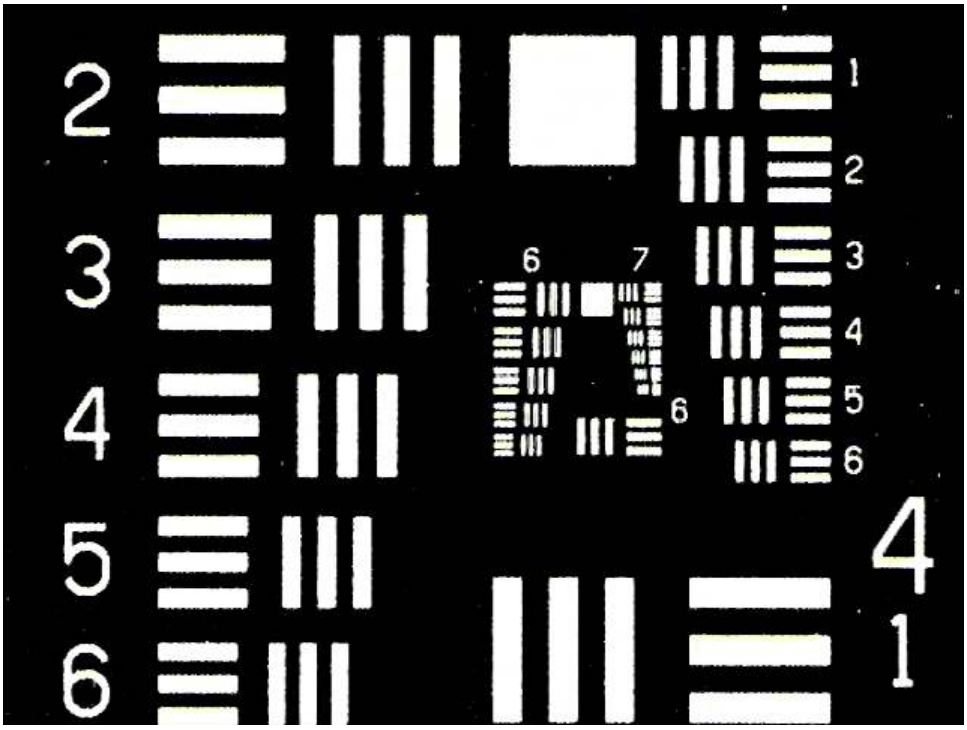


Fig 2.9 – USAF 1951 Optical Resolution Target

which represents 128 cycles/mm. As can be seen in the photo, the vertical lines in this element are easily distinguished, while the horizontal lines are somewhat blurred together. This is a good example of the fact that, for this combination of lens, camera and converter used to make this image, performance is better for vertical edges than horizontal edges. The closely spaced lines in Element # 6 of Group #7 are completely blurred together. From this image, we can say that for vertical lines, the limit of resolution is approximately 143 lp/mm, the spacing in Group #7, Element #2. The limit for horizontal lines, taken from Group #6, Element #6, is approximately 114 lp/mm. This image was acquired by converting one frame of digitized video to a jpeg file. For this study, the vertical lines are of more interest because the scanning will be horizontal, causing the vertical lines to smear together. Any smearing of the

horizontal lines will be due to a combination of video anomalies and stage vibration. Consequently, we will be measuring MTF only for the vertical line pairs.

Suppose that a limit of resolution of 200 lp/mm is desired of a camera. Assume that the microscope's 10X objective is being used to scan for chromosomes. By equation 2.2, the required maximum pixel pitch would be

$$200lp/mm = \frac{1}{2\Delta x} lp/mm . \qquad (2.18)$$

Solving for Δx then,

$$\Delta x = \frac{1}{2 \cdot 200} mm = 2.5\mu m . \qquad (2.19)$$

Therefore, the spacing of the pixels in the CCD chip must be less than or equal to 2.5μm. Any further apart, and the smallest objects in the image will appear blurred together in the image. Here again we are assuming the horizontal spacing and vertical spacing of the CCD are equal. It should be pointed out that the combination of the objective and the camera relay lens together provide magnification of the specimen, meaning that the camera does not have to have 2.5 μm pixel pitch in order for the image to show that much separation. In our system the overall magnifying power is

$$M_T = M_O \text{ x } M_R = 10 \text{ x } 0.45 = 4.5 \qquad (2.20)$$

Where M_T is the total image magnification, M_O is the objective power, and M_R is the power of the eyepiece or **relay** lens. Since we are using the relay lens in the C-tube camera mount, M_R implies the magnification of that lens, which has a power of 0.45X. This magnification of less than 1.0 is necessary to optimally focus the objective's field of view onto the CCD chip. The computer screen can then be used to zoom the image to a greatly magnified size (though not without some loss of sharpness). So, equation 2.10 says that the CCD chip pixel pitch could be 2.5 μm X 4.5 = 11.25 μm and the image would appear to have a limit of resolution of 200 lp/mm. This illustrates the fact that the value of M_T for the microscope and the pixel pitch of the camera together determine the resolution apparent in the final image. The digital conversion process also affects the image quality, with each pixel value represented as an 8-bit quantity. Quantization noise can cause a loss of sharpness.

Another way of checking the resolution in a microscopy system is by use of the stage micrometer, a microscope slide with a ruled line. Figure 2.10 shows an image of a micrometer with a 100 μm ruled line, again using a 10X objective. The smallest markings on the line are at a 2 μm spacing, and can be clearly resolved when viewing the image in the 10X eyepiece. However, the camera/converter system blurs the small lines together, so they appear as a joined dark line. Below the numbers marking the line (the numbers are also blurred) are taller marks that delineate the 10 μm distances, and these lines are clearly distinguishable in the photo. Halfway between the 10 μm marks, are shorter 5 μm lines, and they can also be clearly seen. Therefore, the limit of resolution with this camera and 10X objective is better than 5

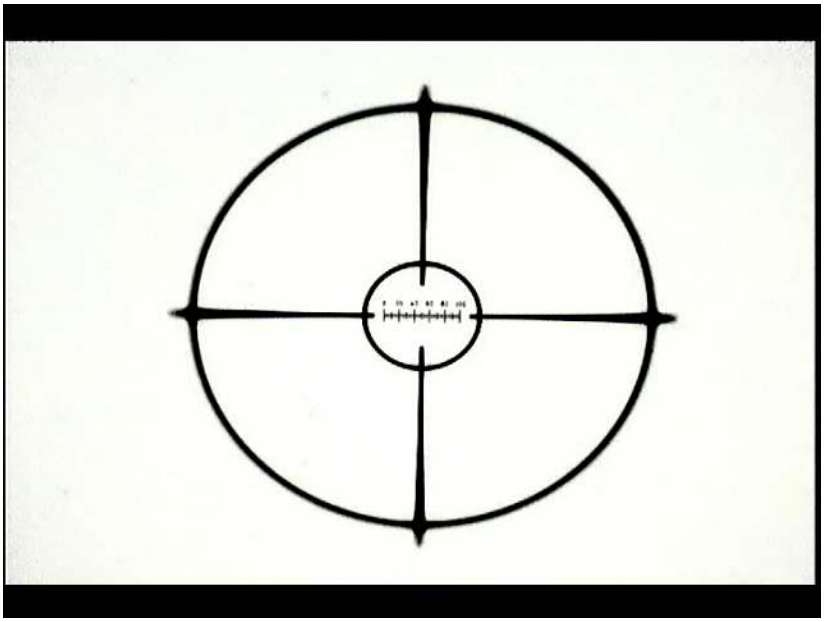


Figure 2.10 – Image of a stage micrometer slide.

μm, but worse than 2 μm. The stagemicrometer is also valuable for measuring the pixel size for a particular system and for measuring features such as a cell or metaphase.

Careful manufacturing techniques are important in order to ensure that the size of each pixel and the separation are uniform throughout the entire surface of the chip. Spatial nonuniformity would cause distortion in the image. The sensitivity of each pixel element, which determines the signal output for minimum detectable light levels, must also be consistent from pixel to pixel for the image to be a faithful representation of the specimen.

Noise, the second critical parameter in a video system, has multiple origins. Quantization noise is due to the fact that each pixel's intensity value is represented by a finite number, usually 8, bits. This means that the digital value assigned to each pixel is only an approximation of the real value. This shortcoming is partly

compensated for by the fact that the human visual system can only evaluate 8 bits worth of video information [43,44]. A computer vision system, on the other hand, might be able to use more than eight bits worth of information, so 12 or even 16 bits worth of information may be valuable in some cases.

At high light levels, quantum noise, which has a Poisson distribution, dominates the system noise. At lower intensity levels, *additive* noise, such as preamplifier noise and readout noise, become more significant.

Readout noise is the tendency for a CCD chip to produce a small digital output even when there are no light photons falling on the pixels. This dark current noise may reduce contrast for low intensity parts of an image. Readout noise will be affected by design choices and temperature, with unwanted impurities in the substrate increasing the amount of noise. CCD detectors are relatively low in noise power, being superior to other digital detectors such as Complementary Metal Oxide Semiconductor (CMOS) detectors or TV *vidicon* detectors. A CCD detector may have a readout noise level of only 12 electrons rms, whereas a conventional TV camera may have a readout noise level of several hundred electrons rms.

For a given light level, the level of the output signal of the device is determined by its quantum efficiency, which is expressed as the number of electrons generated per pixel divided by the number of incident photons. Quantum efficiency varies with the wavelength of the illumination, and is often designed to be highest in the green portion of the visible spectrum, with a wavelength of around 550 nm. This wavelength coincides with the area of maximum sensitivity of the human eye. Typical quantum efficiency for commercial CCD chips is 30% to 70%.

Another important characteristic of a CCD detector is the dynamic range. The dynamic range depends on the readout noise and the well capacity, or well depth, of the silicon substrate. As an example, assume that when saturated with light, a detector element has stored a charge of 78,000 electrons, while in dark conditions, there is a readout noise of 14 electrons. The dynamic range, then, is given by:

$$\gamma = 20\log_{10}(78{,}000/14) = 78db\,. \qquad (2.21)$$

Ultimately, the quality of an image can be related to the signal-to-noise ratio, and any source of noise can cause the SNR to be negatively impacted. Therefore, even if a CCD chip has excellent pixel pitch and sensitivity, noise sources may make the actual quality worse than hoped for. The actual SNR is very difficult to measure in an imaging system. Therefore, an alternative, but related, measurement is used to measure image quality. It is called the modulation transfer function (MTF). It relates the intensity modulation, or distortion, caused by the components of an imaging system. The MTF is actually a normalized Contrast Modulation Function (CTF) where the maximum MTF is assumed to have a value of 1.00. The formula for calculating the CTF is given as:

$$CTF = \frac{I_{\max} - I_{\min}}{I_{\max} + I_{\min}} \qquad (2.22)$$

where $I_{\max}$ represents the intensity level of the maximum bright spots and $I_{\min}$ represents the minimum intensity level in the image.

The basic idea is to have a known target object, with very high contrast and known line spacing imaged by the system under test. The loss of contrast in the image is what generates the value of the MTF. MTF is, then, a percentage of contrast in the image compared to the known contrast in the target. The value of MTF tends to get worse as the line spacing in the target gets smaller, and so MTF is usually graphed as a function of lp/mm. Finally, when the value of MTF goes to zero, meaning that the lines can no longer be separated in the image, the lp/mm at that point is considered to be the **limit of resolution** for the system. In an imaging system, the MTF of the resulting image is the product of the MTFs of the individual components of the system.

Equation 2.12 is the method of calculating CTF. If the USAF target is used to measure MTF, which is the normalized CTF, in an imaging system, the equation is solved for each of the groups and elements in the target, and those values are graphed versus the line spacing. As shown in Figure 2.11, the ideal MTF curve shows an MTF smoothly decreasing as the line spacing gets closer, in a somewhat Gaussian fashion. MTF can be seriously degraded by motion blur. In a video scanning system where the stage is constantly in motion during video capture, the motion blur will cause the contrast between adjacent structures to be severely reduced. Thus, an MTF curve for a full motion image will generally be lower than for a still image of the same object. In the idealized MTF plot in Figure 2.11 each curve represents a different rate of scan speed. As the scan rate increases, the MTF is reduced, making the features in the image blur together. Figure 2.12 shows the USAF target imaged during a full motion scan of approximately 5 mm per second horizontal motion.

Comparing this image of the target with that in Figure 2.9 shows the severe blurring caused among the smaller line pairs.

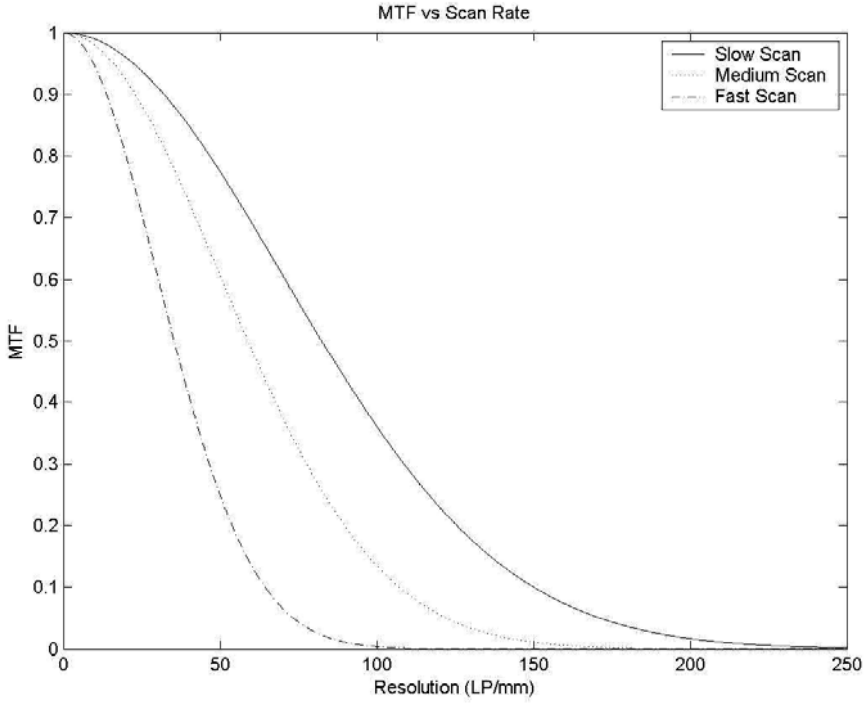


Fig 2.11 – Idealized MTF Curves for Scanning

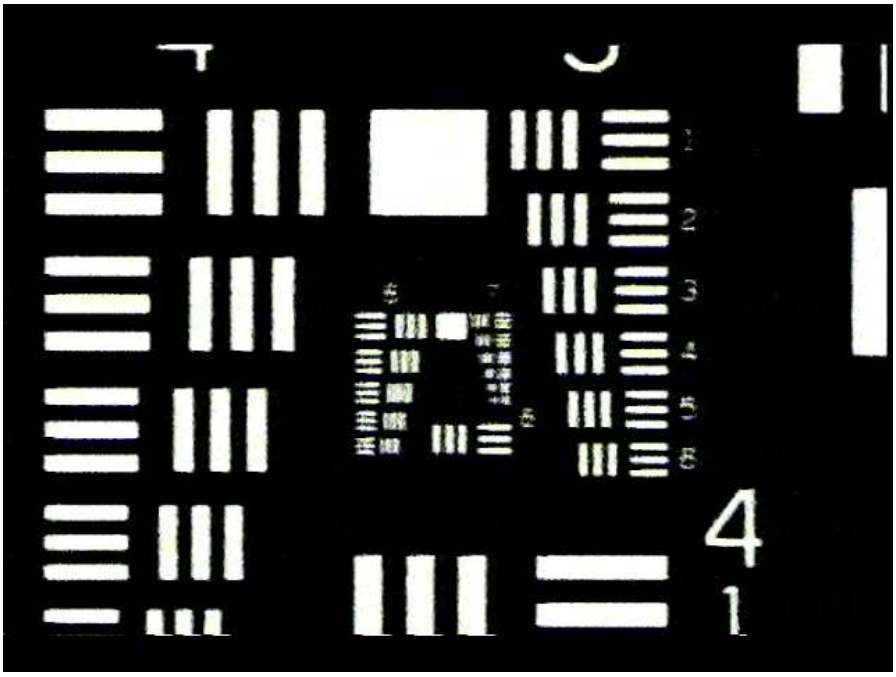


Fig 2.12 – USAF Target Under Motion Scan

The MTF of a 2D image can be related to the so-called *point-spread function* (PSF), a way to characterize the way that light passing through a pinhole spreads out as it exits the hole. The MTF is actually the Fourier Transform of the PSF. The relationship is shown in the following formula:

$$MTF(u,v) = \iint PSF(x,y)e^{j2\pi(uv+xy)}dxdy \qquad (2.23)$$

where u and v represent spatial frequency in the horizontal x and vertical y directions, respectively. An alternative way to calculate the MTF is by transforming the *line-spread function* (LSF),

$$MTF(u,v) = \int LSF(x)e^{-j2\pi ux}dx \qquad (2.24)$$

The LSF is the result of light passing through a narrow slit. These two equations show that MTF is a function of spatial frequency. Because it may be difficult to derive the LSF for an optical system, measuring MTF by means of the CTF is usually more practical.

In order to derive meaningful measurements of MTF, a method had to be arrived at that would take into account some of the difficulties that exist when the stage is moving. For example, the CTF formula requires that minimum and maximum pixel values be measured at the line pairs. This may sound simple, but in fact the pixel values typically vary over a range on either side of a given line pair. Measurement of a randomly chosen pair of pixels at the line pair may produce a relatively high CTF value, whereas a different pair of pixel values for the same line pair may produce a much lower CTF. At the same time, if the brightest pixel is searched for and selected for the Imax value, and the darkest pixel is selected for the Imin value, this might also produce an unrealistically high MTF. In order to allow for this variation and still give a meaningful value, we average all of the "bright" pixels (those whose values are in the upper 50^{th} percentile of pixels) to derive the Imax value, and we average the "dark" pixels (those whose values are in the lower 50^{th} percentile of pixels). This method, while somewhat arbitrary, tends to give a more repeatable and useful value for the CTF, and hence, the MTF.

The procedure for measuring the MTF requires that a video frame be extracted from the scan and saved as a still image JPEG file. A few of the frames will show the

center of the USAF target, with the smallest groups approximately centered in the frame. The microscope will be manually adjusted to achieve the sharpest possible image. The PC software will then be started in the capture mode and a few seconds of video stored in a multiframe video file. One of the frames will be then be extracted from the file and used for the measurements. When using the USAF target, the slide holder is removed from the stage and replaced with a glass plate. The target is then placed on the plate and properly oriented. The light from the microscope's light source comes up through the plate and into the target, allowing good contrast for the target's image.

For a motion scan, the target is first centered vertically in the frame, and the image is adjusted for proper focus with the desired objective lens in place. The stage X axis motor is set to run at the desired speed and the video software is cued for image capture. The stage is then instructed to move a centimeter or so horizontally, while maintaining its vertical (Y axis) setting. With the stage set to run in the X direction at the desired speed, the video capture is started and the X axis motor instructed to move towards, and a little beyond, the target. This method ensures that the motor speed is constant as the target passes under the objective lens. For subsequent scans, the same procedure is used, with the X axis motor speed adjusted as required. After the desired scan speeds have been completed, the entire procedure is repeated with different objective lenses in place until all combinations of scan speed and lenses have been tested.

As soon as the stage completes the scan, the video capture is stopped, and the video file is opened for frame extraction. The frames are viewed individually, and

one frame will be selected that shows the smallest groups approximately centered in the frame. The frame is then saved in JPEG format for further processing. A utility program was written that opens the JPEG file and renders the image on the PC screen. Using the mouse, a rectangle is drawn within each of the linepairs to be used in the MTF measurements. The program then uses the rectangular areas to make the calculations of the contrast. As state previously, the vertical linepairs are used because the horizontal motion causes the vertical lines to blur together, allowing for a meaningful MTF measurement. The utility program then calculates an average of the dark pixels and an average of the light pixels and performs the CTF/MTF calculations for each line pair. The values can then be graphed, with the horizontal axis of the graph representing the resolution, or lp/mm. The smallest 24 linepairs are sufficient for the graph because the MTF for larger linepairs is essentially 1.0, even with a motion scan.

Fig 2.12 shows the way that MTF varies with the scan rate for the X10 objective lens. Three different scan speeds were used. One is a still image, where the scan speed is zero, and the other two are at 1mm/sec and 2mm/sec. Fig 2.13 shows one frame from the video where the stage is not moving, a scan rate of zero. Fig 2.14 shows a frame with a scan rate of 1 mm/sec, and Fig 2.15 shows one frame from a 2 mm/sec scan. It can be seen that the blur in the smaller vertical linepairs is worse for the 2mm/sec scan than for the 1mm/sec scan, and the still image has the least blur.

After the MTF values are calculated, data are connected in a smoothed plot by using a polynomial method. As expected, the general trend of the data is that the MTF will fall off as the lp/mm gets larger, and that the faster the scan rate, the more

quickly the MTF falls. The limit of resolution, the point where the MTF drops to zero, is much better than 250 lp/mm for a still image, but only about 200 lp/mm for the moving scans. It can be seen that the MTF values does not fall off in a continuous Gaussian curve, even after the smoothing. This anomaly is due to imperfections in the optics and camera used

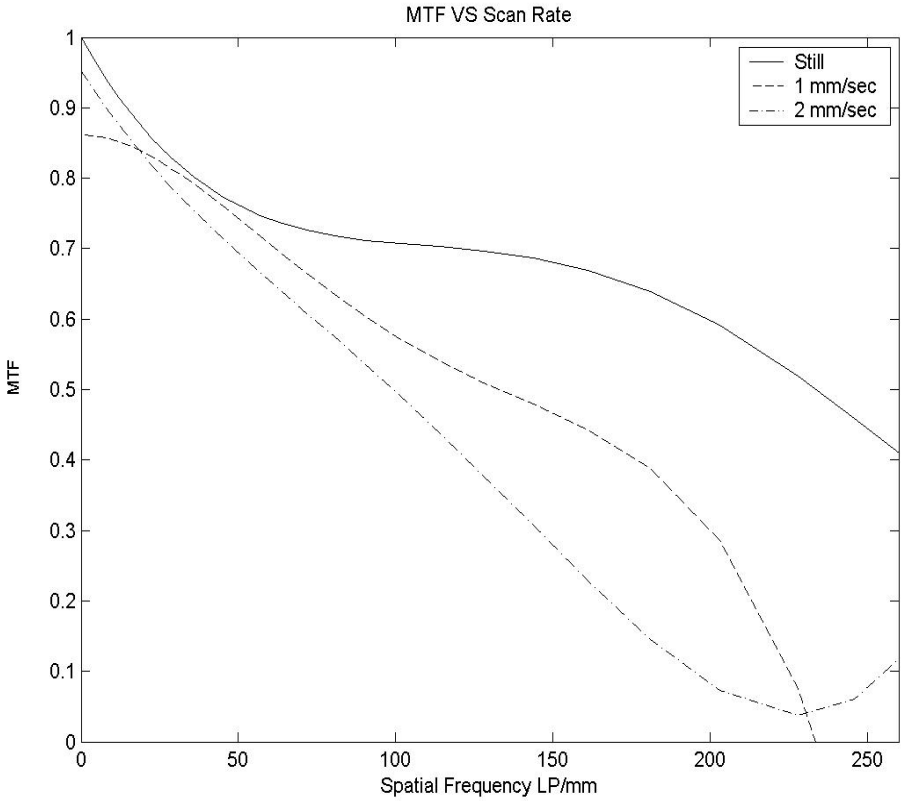


Fig 2.13 – MTF for three scan rates using a 10X objective lens

to make the image. Primarily, it should be kept in mind that focus is optimum at only some parts of the image, usually better in the center, but may vary from place to place. In fact, during a motion scan, the anomalies may cause the MTF to actually be better for a smaller segment than for a larger one nearby. In order to correct for this

error, multiple scans could be made, and the average MTFs at each resolution calculated and graphed. However, a single run is sufficient to reveal the general effect of scan speed on the MTF.

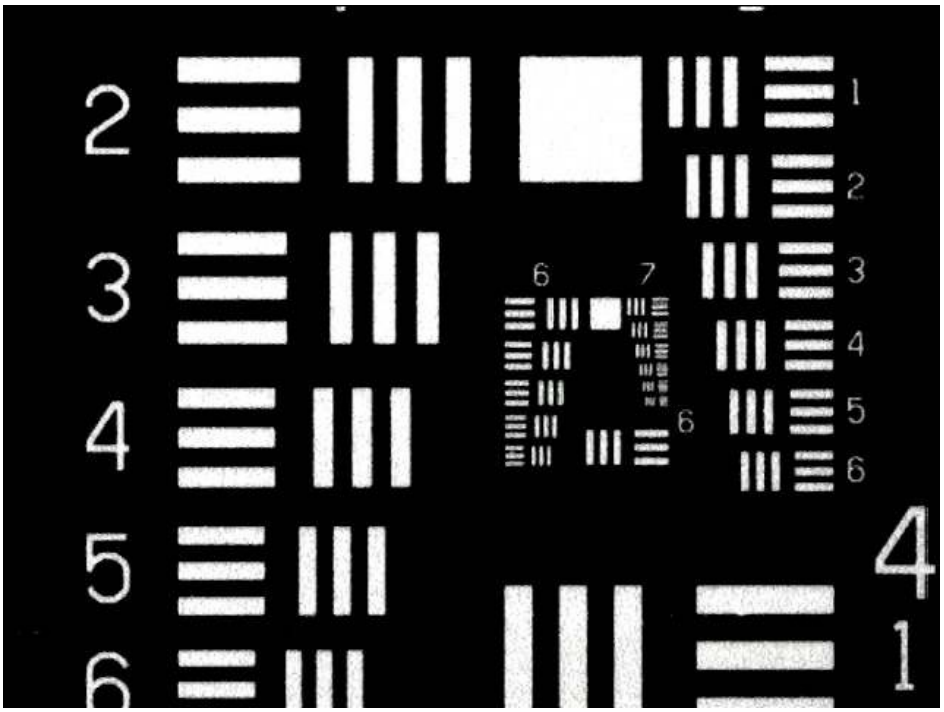


Fig 2.14 – USAF target still image with 10X objective lens

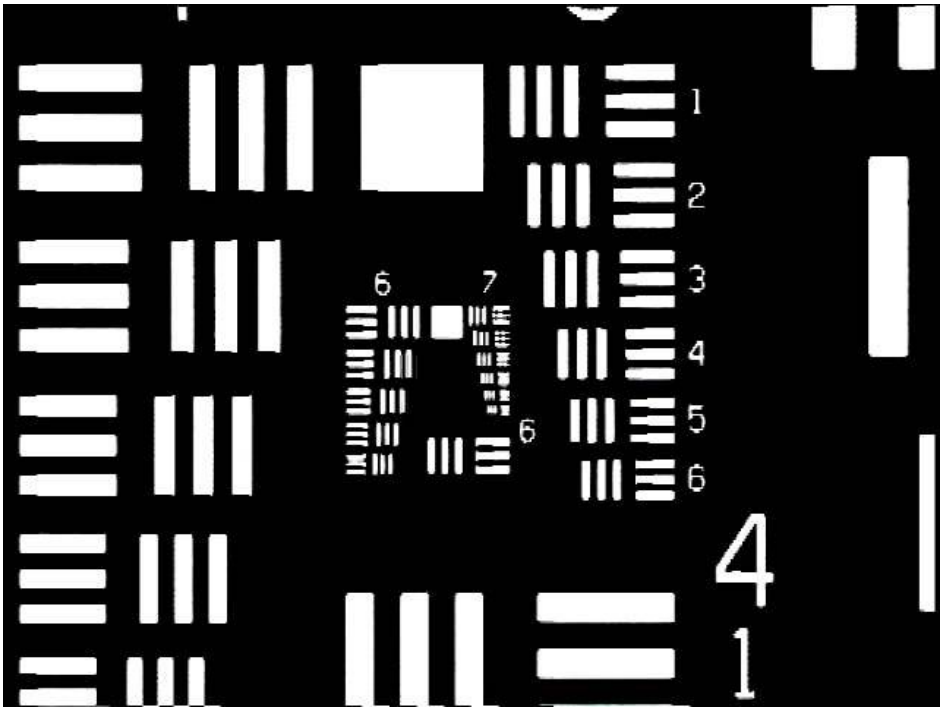


Fig 2.15 – USAF target with scan rate of 1 mm/sec and 10X objective lens

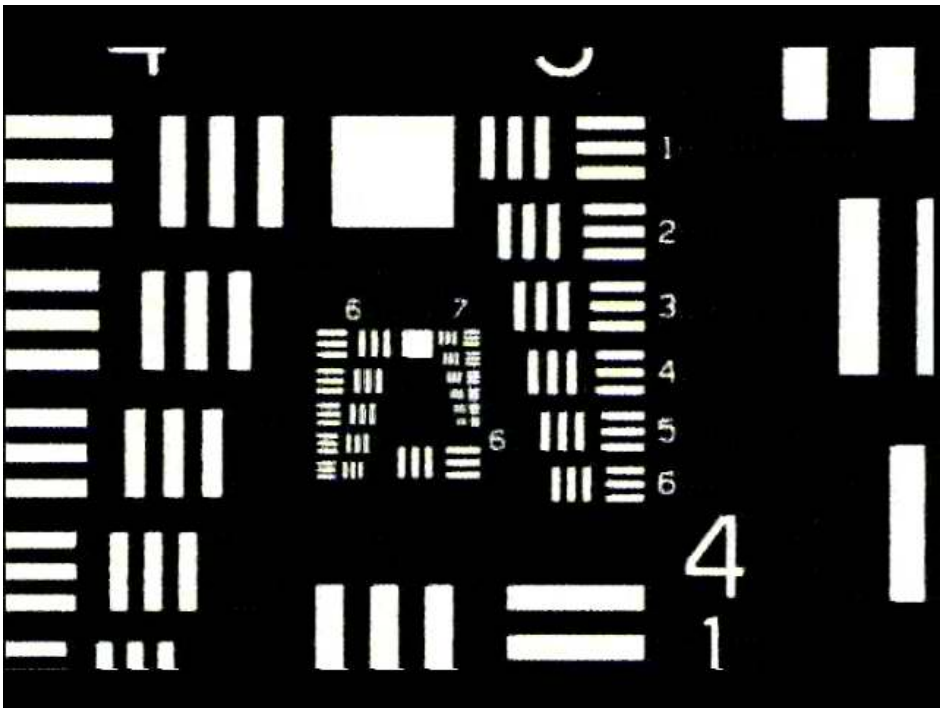


Fig 2.16 – USAF target with 2 mm/sec scan with 10X objective lens

Fig 2.16 shows the MTF graph for the same scan speeds, but using a 20X objective lens. Fig 2.17 shows one frame from the still image, while Figs 2.18 and 2.19 show frames from the 1 mm/sec and 2 mm/sec scans. For a still image, the resolution is quite good using the 20X lens, giving twice the magnification of the 10X objective. The higher resolution can be seen in the MTF for the still image. At the right end of the graph, the MTF for the solid line is around 0.64, whereas Figure 2.12 shows the MTF at 0.42 at the same point for the 10X objective. For the 1 mm/sec scan, the MTF maintains a high level for smaller resolutions, drops rapidly above 200 lp/mm, but still does not reach zero. However, for a scan rate of 2 mm/sec, the MTF drops off very quickly, reaching zero around 150 lp/mm.

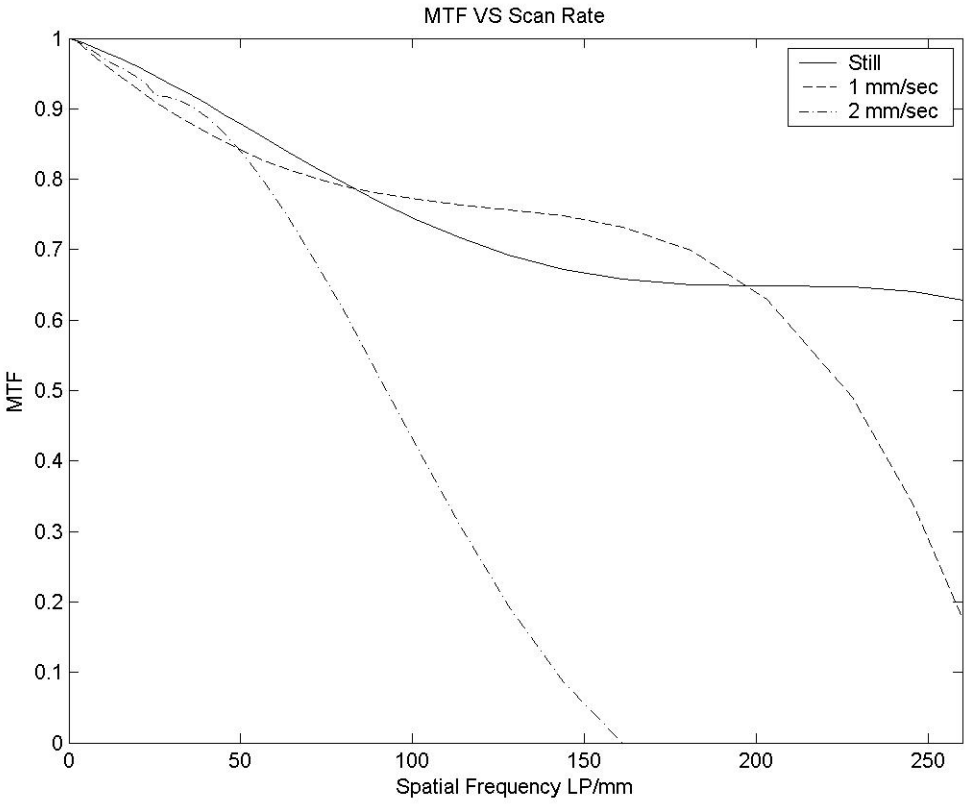


Fig 2.17 – MTF curves for 20X objective lens

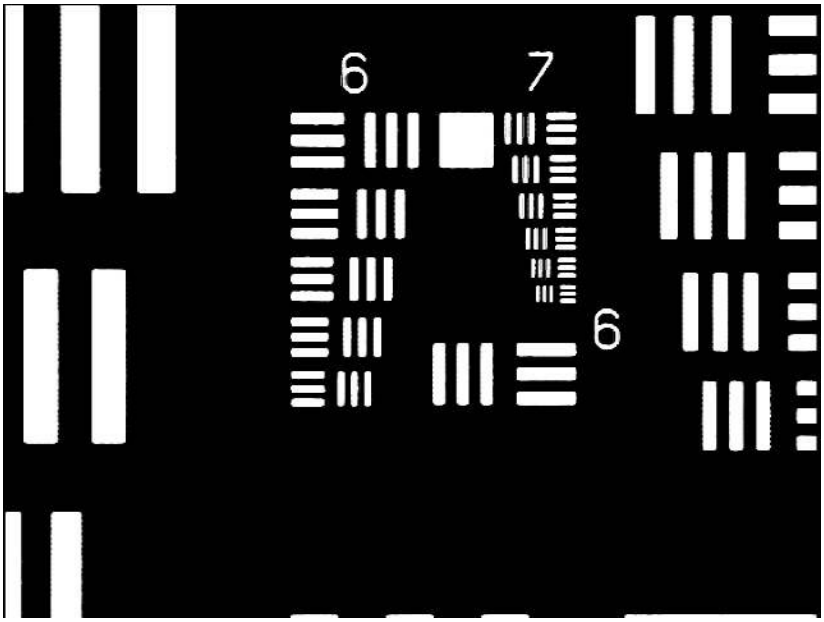


Fig 2.18 – USAF target still image with 20X objective lens.

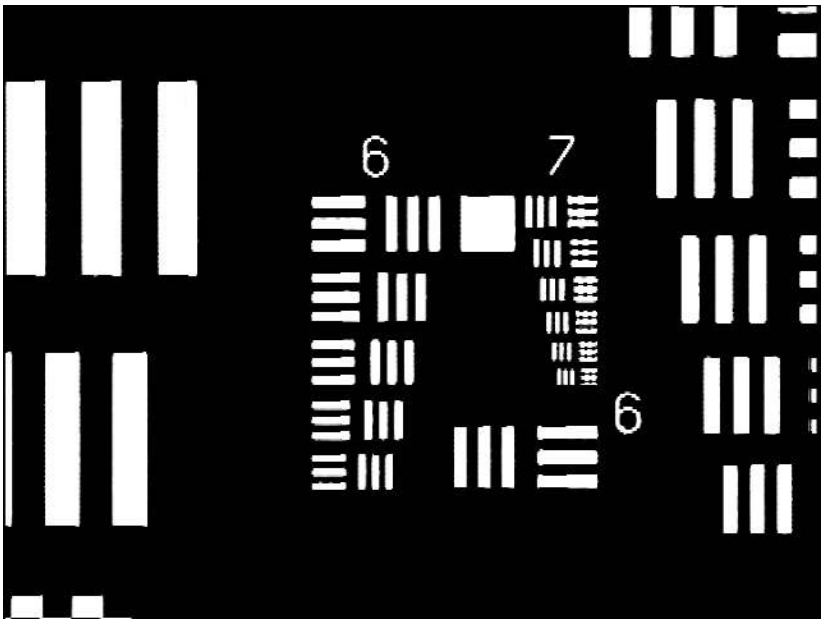


Fig 2.19 – USAF target with 1 mm/sec scan rate and 20X objective lens

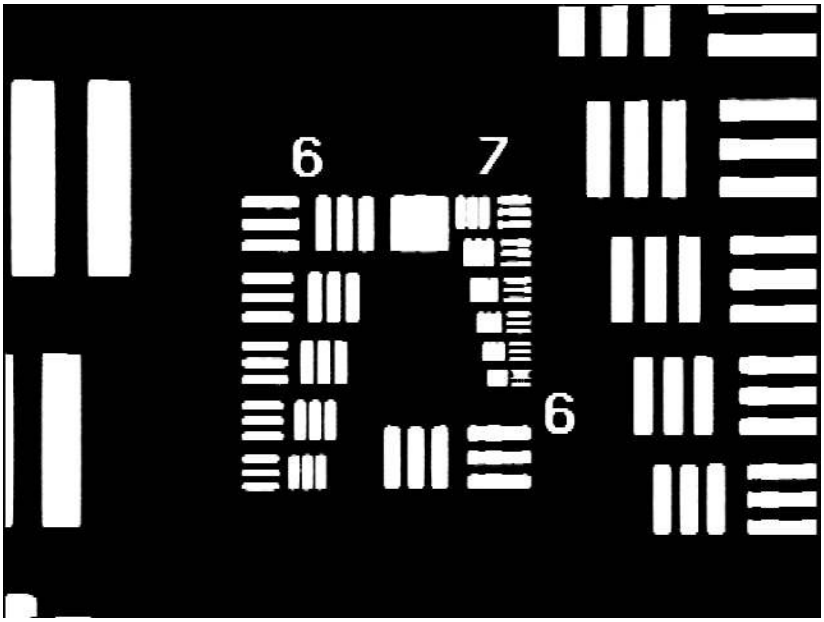


Fig 2.20 – USAF target with 2 mm/sec scan rate and 20X objective lens

Fig 2.20 shows the graph for the 40X objective lens, with the same scan rates as before. Fig 2.21, 2.22, and 2.23 show the frames of the target at the speeds corresponding to the scans. As expected, the sharpness is excellent for the still image. The MTF is 0.8 or better for the majority of the linepairs. For the 1 mm/sec moving scan, however, the blur is so severe that the vertical linepairs are completely blurred for the nine smallest segments. The smaller field of view at the higher magnification level causes the motion blur to be much worse. In fact, the MTF drops to zero almost immediately at 1 mm/sec scan rate. At 2 mm/sec scan rate, the target is essentially unrecognizable.

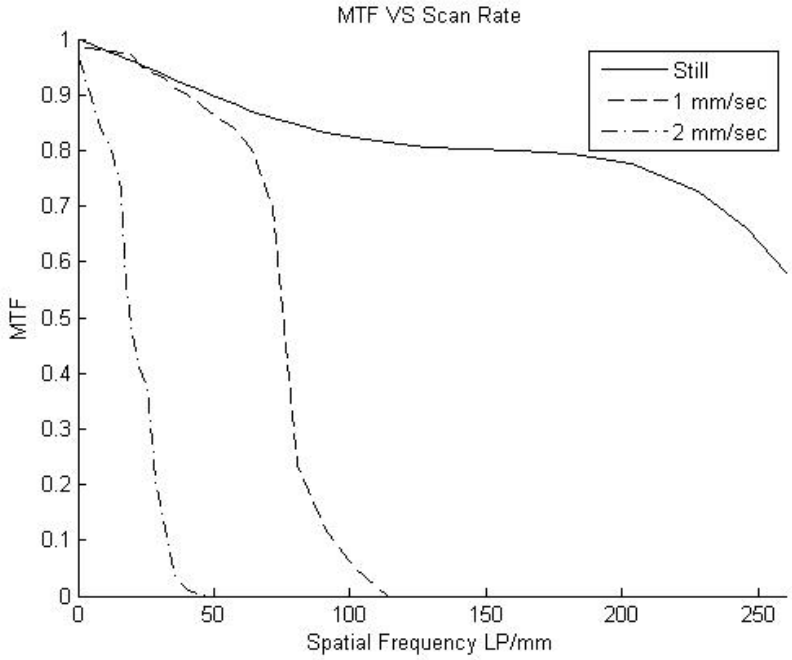


Fig 2.21 – MTF curves for 40X objective lens

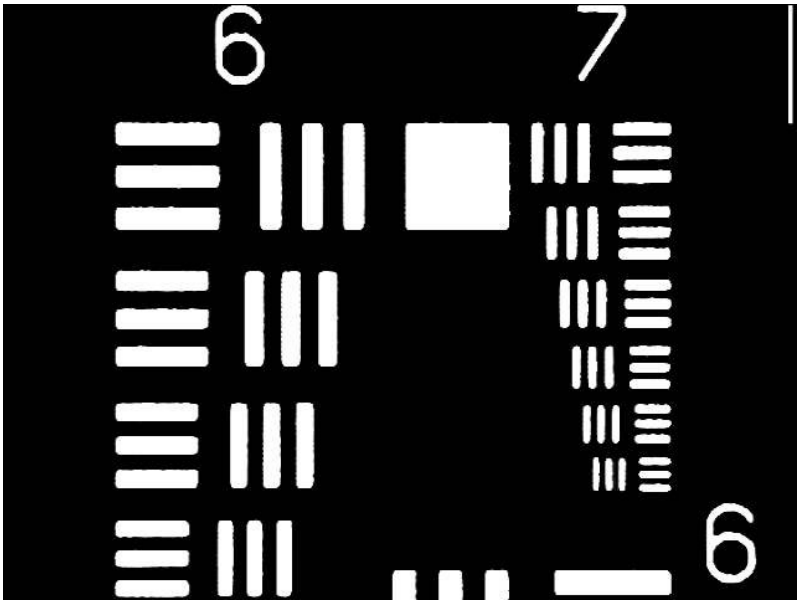


Fig 2.22 – USAF target still image with 40X objective lens

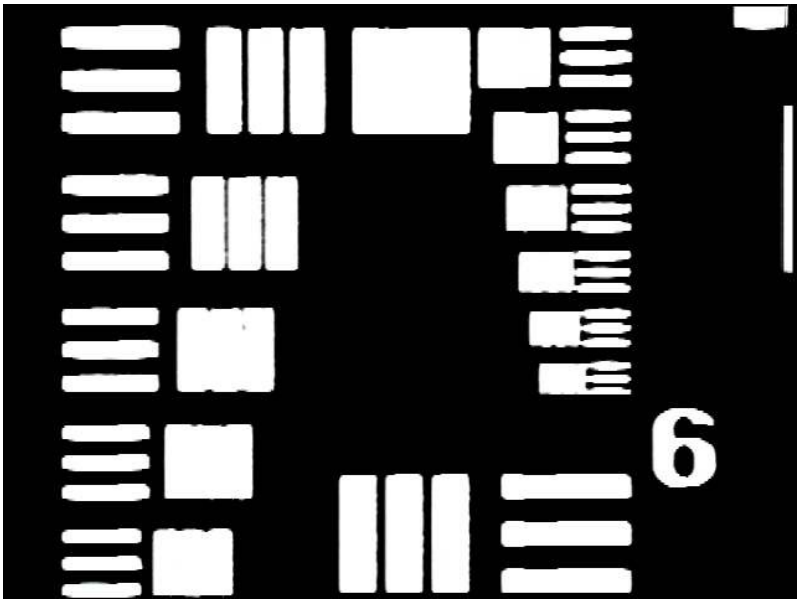


Fig 2.23 – USAF target with 1 mm/sec scan rate and 40X objective lens

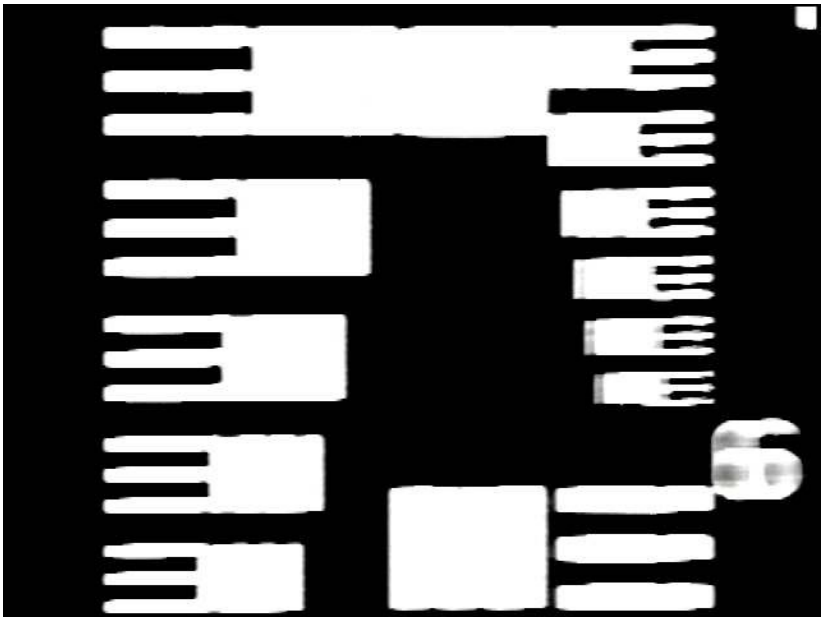


Fig 2.24 – USAF target with 2 mm/sec scan rate and 40X objective lens

The effect of scanning speed on the MTF shows that using a high level of magnification can be counterproductive. The better resolution in the still image is no longer an advantage when the scan rate is high. The image quality quickly deteriorates once the image begins to move. It is relatively easy to explain why the blur is so much worse with the smaller field of view under high magnification. When the slide is not moving, the light reaching a single pixel element on the CCD chip during one frame is relatively constant. The pixel element receives light from only one small spot on the image. As stated previously, this spot is approximately 3.5 μm when using the 10X objective. However when the stage is moving horizontally, the light reaching a pixel in the CCD chip is not constant. The light comes not from just one small 3.5 μm spot, but

from several such horizontally contiguous spots which pass under the objective lens during the frame. The light reaching the pixel during the frame can represent the average intensity of a horizontal strip of the image, rather than the exact value of those pixels. Depending on the spatial frequencies in the image, this average intensity can be quite different from the actual value. High spatial frequencies represent edges or abrupt changes in texture, and these details will be smoothed over and blurred by the scanning motion.

A numerical example helps to illustrate this averaging process. Suppose that in a still image a pixel on the CCD chip receives the light from a spot on the slide that is 3.5 μm X 3.5 um. With a horizontal stage motion of 1mm per second, and a frame rate of 30 frames per second, the distance the stage moves during one frame is found as follows:

$$dist = \frac{1mm/\sec}{30\,frames/\sec} = 33\frac{\mu m}{frame} \qquad (2.25)$$

Therefore, during the time of one frame of video, 33 μm of the image will pass under each pixel element in the CCD chip. To determine the number of image pixels that contribute light to a single CCD pixel during the frame, we divide the above value by the width of the CCD pixel, as follows:

$$\#\,frames = 33\frac{\mu m}{frame} \div 3.5\frac{\mu m}{pixel} = 9.5\,pixels \qquad (2.26)$$

Therefore, assuming that the CCD is storing photons during the entire 33.3 msec frame time, the light from at least nine image pixels will contribute to each CCD pixel value. This averaging process will smooth the image as if an averaging filter had been applied to the values. Details in the image will be lost and edges will be spread out to a greater width.

The above equation shows that the smaller the field of view, which corresponds to a higher magnification power in the objective lens, the more image pixels will contribute light during each frame. Therefore, a pixel size of 3 μm would smooth the intensity of 11 contiguous image pixels, and so forth. The amount of smoothing, and thus blurring, gets worse and worse as either the scan rate or the magnification power increases. For this reason, the scan speed must be limited to a rate which preserves the image features which are of interest. A metaphase spread, with a diameter of approximately 50 μm, can be scanned at a rate in excess of 1mm/sec with an objective power of 10X, incurring only modest loss in essential detail. On the other hand, an individual chromosome scanned at the same rate, requiring an objective power of 60X, would suffer significant blur, making the image unusable. At high magnification levels, where extremely small features are of interest, the scan speed would have to be reduced to a level that would require scan times of unacceptable length. Even though the MTF for the 20X lens is still relatively good at a 1 mm/sec scan rate, the smaller field of view means that it takes longer to scan the slide than it does with a 10X lens. Therefore, we can conclude that it is best to search for metaphase spreads using an objective power of 10X and rely on visual methods or digital pattern recognition algorithms to identify the spreads, then image

the chromosomes under higher magnification in a still image. In this manner, the entire scan can be performed in 15 minutes or less, with the spreads found with a search algorithm, while the next slide is being imaged.

Chapter III – Motion Scanning of Metaphase Spreads

Section 3.1 – Visual Appearance of Scanned Metaphases

The purpose of the scanning system is, after all, to quickly scan a slide and recognize the metaphase chromosomes. The 1951 USAF target provides a way to quantify the image quality, allowing us to compare different scan speeds and objective powers. These measurements will be merely academic if there isn't also a comparison of scan rates and powers for the human visible metaphase images. In other words, what is the effect of the scan rate and power on the successful recognition of a metaphase? In this chapter, the scanning of actual metaphase cells will be discussed, and the results of metaphase scanning will be related to the MTF measurements described in the previous chapter.

It is informative to compare the obvious distortion of the line pairs in the target to the distortion seen when a metaphase is scanned. Figure 3.1 shows a frame from a 2 mm/sec scan of a metaphase, using a 10X objective lens. Perhaps surprisingly, the telltale features of the metaphases and other cell material are still quite visible, in spite of the loss of resolution. As a further comparison, Fig 3.2 shows the USAF target scanned at 8 mm/sec. While it is difficult to distinguish the smaller line pairs, it is still easy to tell that the image represents the target, albeit badly blurred. What appears to allow the visual recognition is the fact that both the target and the metaphase are "feature rich", meaning that there are multiple features in different orientations, making the overall image stand out from the background [46-

49]. If it were necessary to recognize a single chromosome, instead of an entire metaphase spread, a much smaller amount of blur would be tolerable.

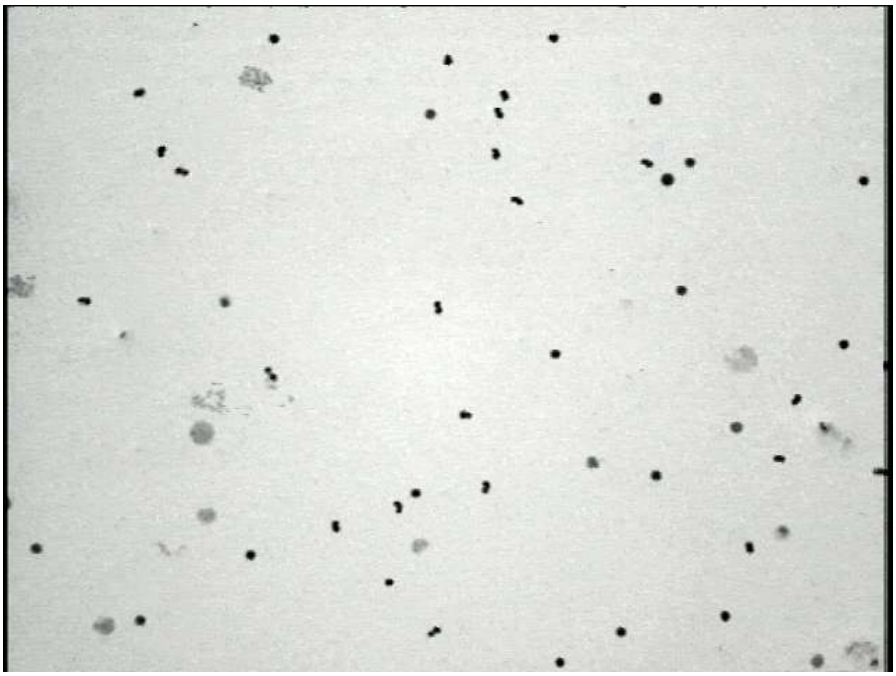


Figure 3.1– Slide scanned at 2 mm/sec using 10X objective lens.

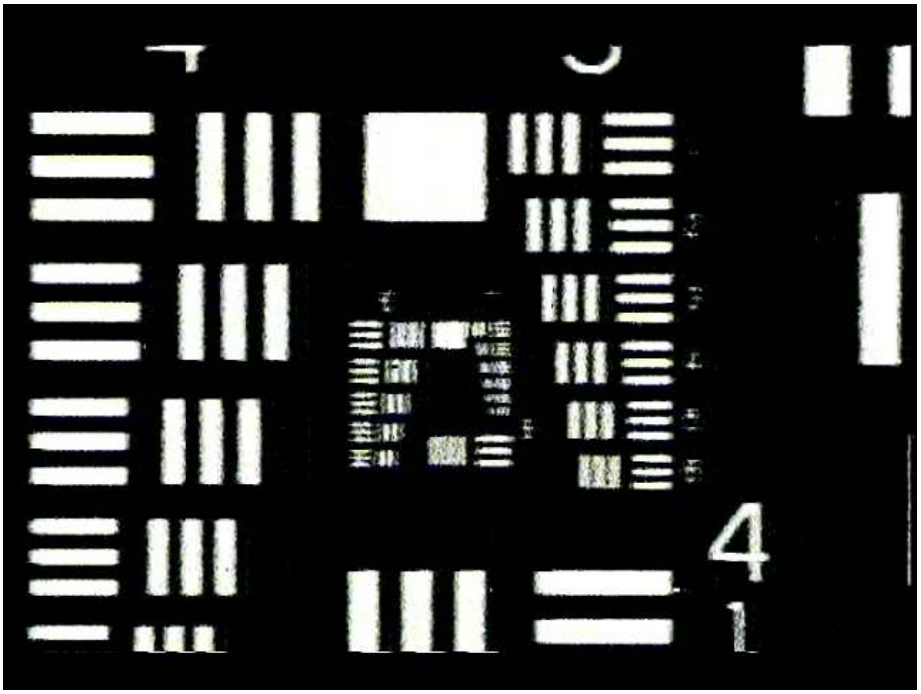


Fig 3.2 – USAF target scanned at 8 mm/sec using 10X objective lens.

In order to do a more exact comparison, Figure 3.3 shows a still image of another metaphase grouping, using the 10X lens. There is one rounded metaphase in the upper left quadrant of the image, and another grouping in the center. The center grouping is shown highly magnified in Fig 3.4, using the 60X lens. The distinctive shape of the grouping, as well as the individual chromosomes, can be seen quite clearly at this magnification. This metaphase would be an excellent candidate for karyotyping because the chromosomes show minimal overlap.

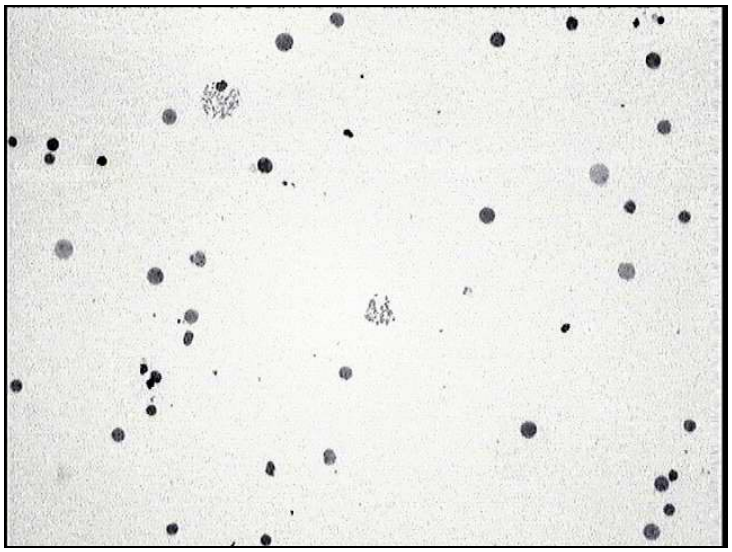


Fig 3.3 – Still image of metaphases using a 10X objective lens.

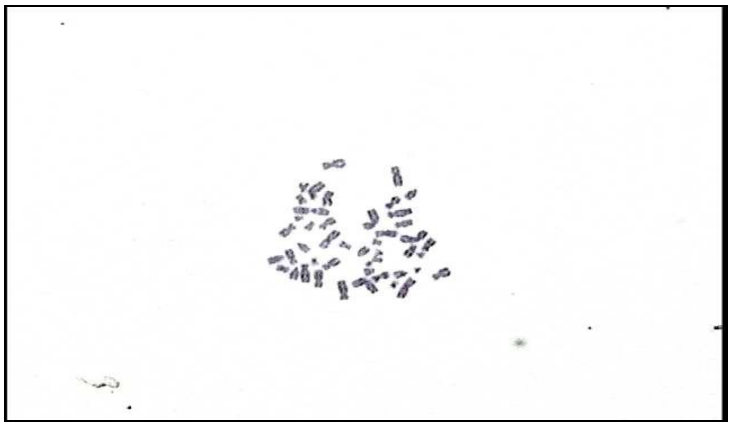


Fig 3.4 – Still image of the center metaphase using the 60X objective lens.

Figure 3.5 shows the same image captured at a horizontal scan rate of approximately 1mm/sec with the 10X objective lens. Motion blur is evident. The chromosomes have begun to merge together, but the metaphases can still be visually identified. In

Fig 3.6, at 2mm/sec, the blurring effect is quite pronounced and the image quality has deteriorated significantly. A trained observer can still recognize the presence of the metaphases, but it is far more difficult to tell whether they would be suitable for the karyotyping process.

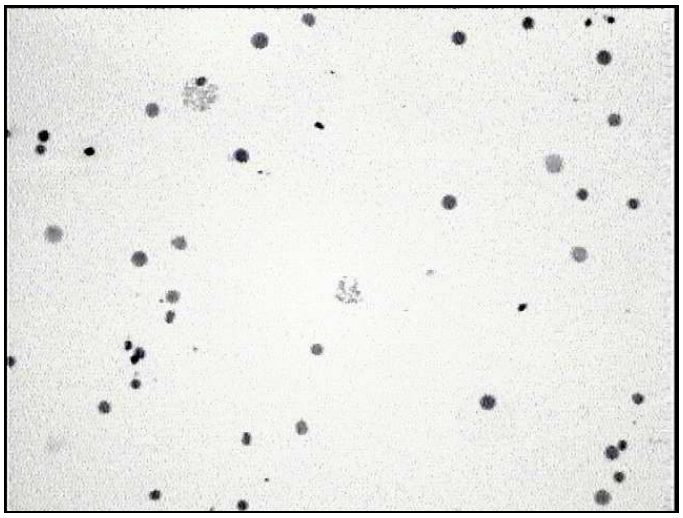


Fig. 3.5 – Image captured with 1mm/sec scan rate.

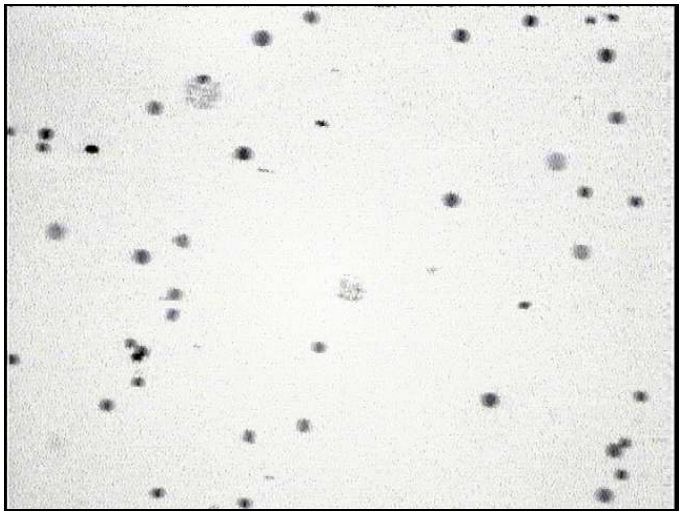


Fig. 3.6 – Image captured with 2mm/sec scan rate.

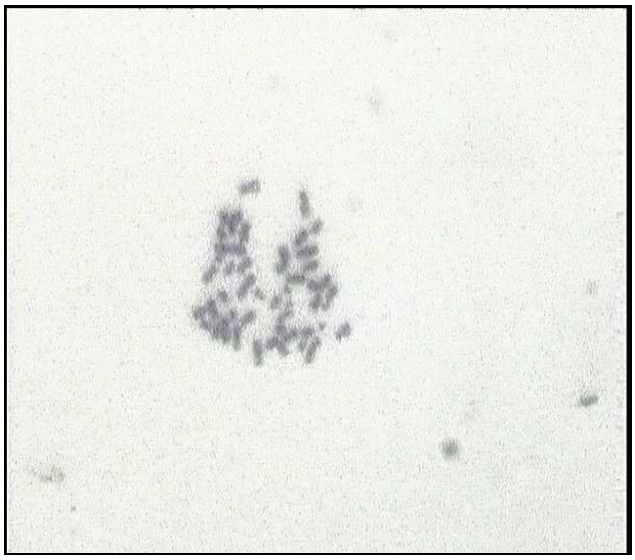


Fig. 3.7 – Image captured with 1mm/sec scan rate, using the 60X objective lens.

In order to show the effect of scan rate on the metaphase patterns, Fig 3.7 shows the same metaphase at a 1 mm/sec scan, using the 60X objective. The overall shape of the metaphase is still apparent, but the individual chromosomes are no longer sharp and clear. The edges are smeared. Still, since the metaphase is easily recognized, it could be said that scanning with the 60X objective at this scan rate might still be advantageous. The problem with this method is that the field of view is so small that the time to scan the entire slide at this magnification is extremely long, taking well over one hour. Figure 3.8 shows that with a scan rate of 2mm/sec the 60X objective lens magnification produces an image with little more than smudges. This result is similar to what is seen in the MTF measurement graphs, where the blur at 2 mm/sec scan speed was much worse than that at 1 mm/sec at higher magnification.

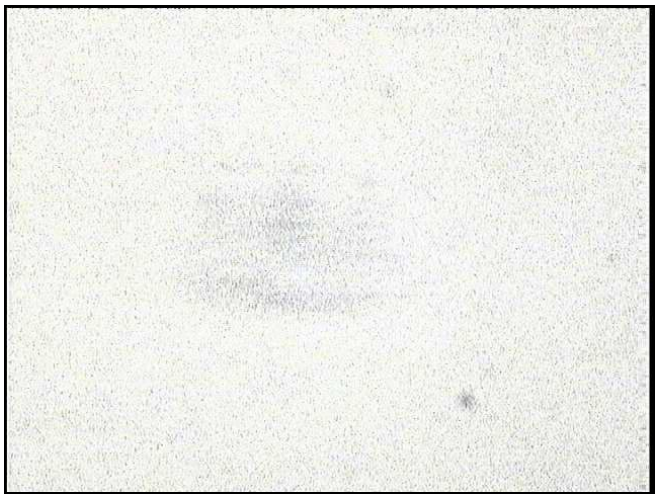


Fig. 3.8 – Image from Fig 3.7 captured at 2mm/sec scan rate.

The problem of motion blur emphasized the importance of frame rate for the video system. Our video system captures video at the relatively slow 30 fps rate. A higher frame rate would reduce the loss of detail in the image. Clearly, if we wish to scan the slides quickly, a higher frame rate video system would be desirable. frame rate and image quality. Once again, it may be possible for the image processing software to deal with the motion artifacts when performing pattern recognition; it will reduce the system's effectiveness if the operator sees a poor quality image which is blurred.

Section 3.2 – Metaphase Finding

Metaphase finding is essentially a pattern recognition problem, where one or more features must be identified so that a decision can be made as to whether a metaphase is present within an image [46]. If enough of the features are present, then a decision can be made based on some predetermined criteria. The identifiable features of a metaphase will depend on the objective lens power being used. At high

magnification, the individual chromosomes can be measured and counted, giving two features to use in making the decision. However, at 10X objective power, the chromosomes are not usually very distinct and so cannot be easily measured or counted. Another feature must be searched for.

The most noticeable feature of a metaphase under 10X objective power is the *texture*. There are a number of different techniques for detecting a particular texture, such as Gabor filters and other filters based on measurement of the spatial frequencies along certain directions. These techniques try to emulate the way in which a human or animal brain is thought to detect textures [45,50]. One of the simpler methods of finding textures uses a so-called gray-level co-occurrence matrix [43]. The co-occurrence matrix method uses a window to acquire a group of statistics about the texture being tested. The statistics are then used to populate the co-occurrence matrix. From the matrix, different measures of texture can be calculated. The four most useful ones for metaphase detection are entropy, energy, contrast, and homogeneity. When these values are calculated, they can be compared with limits which have been obtained from training data. The algorithm will then signal that the sought for texture has been found if the three measures fall within the limits. A searching algorithm would also identify the coordinates of the found pattern within the overall image by using the frame number of the video, or by querying the stage if the finding is being done in real time.

Any number of gray-levels can be used in populating the matrix, but the size of the matrix is equal to N^2, where N is the number of levels. Since the computation time is determined by the size of the matrix, it is desirable to limit the number of

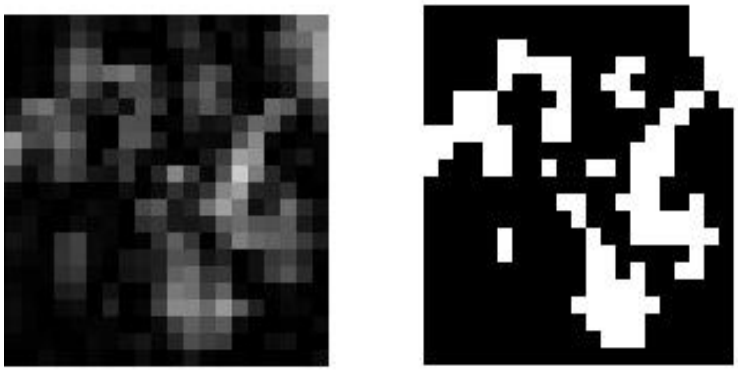
levels to the minimum needed to classify or segment the texture. If working with a binary image, there are only two gray levels, so the matrix is 2x2 in size. This size greatly reduces the computing time.

For a 2x2 co-occurrence matrix, the measures of texture can be calculated using the following procedure:

- Perform background subtraction and contrast stretching.
- Convert the image to binary using suitable threshold level.
- A window which will cover the texture pattern is passed over the image.
- A displacement vector **d** = (d*x*,d*y*) is chosen to define which pixels are paired.
- Within the window, the relative values of the paired pixels are sorted into bins.
- The matrix, P[i,j], is populated with the totals in the bins.
- The entropy is calculated as: Entropy = $-\Sigma\,\Sigma\, P[i,j] \log P[i,j]$.
- The energy is calculated as: Energy = $\Sigma\,\Sigma\, P^2[i,j]$.
- The contrast is equal to: Contrast = $\Sigma\,\Sigma\, (i-j)^2 P[i,j]$.
- The homogeneity is found by: Homogeneity = $\Sigma\,\Sigma\, P[i,j] / (1+|i-j|)$.
- If these values satisfy the chosen limits, the texture has been recognized.

As an example, we can choose a window that is large enough to cover most of a typical metaphase. Measurements show that a 21 X 21 window will cover most of

the texture. Figure 3.9 shows the gray-scale and binary representations of the window over a metaphase. Figure 3.10 shows the numerical values of the binary image inside the window. For an initial value of **d** = (dx,dy), we can choose (1,1),



(a) Grayscale (b) Binary

Figure 3.9 – The 21 x 21 window segmenting a metaphase.

which means that the pixels of the pair are diagonally connected, as shown in Figure 3.10. The figure also shows the values in the matrix resulting from processing the 21 x 21 window. Since there are $(21 - 1)^2 = 20^2 = 400$ pairs of pixels with a (1,1) spacing, the values in the matrix are normalized by dividing each value by 400. Now the algorithm counts the instances where pixel i and its paired pixel j, one pixel to the right, and one pixel down, have binary values (0,0), (0,1), (1,0), or (1,1). The totals for each of these pixel value combinations are entered into the corresponding row and column of the matrix. This result is not surprising, inasmuch as most of the metaphase is dark, and the white areas are clumped together.

0	0	0	0	0	0	0	0	0	0	0	0	0	0	0	0	0	0	1	1	1
0	0	0	0	0	0	0	0	0	0	0	0	0	0	0	0	0	0	1	1	1
0	0	0	0	0	1	1	0	0	0	0	0	0	0	0	0	0	0	1	1	1
0	0	0	0	0	1	1	1	1	1	0	0	0	1	1	0	0	0	0	1	1
0	0	0	0	0	1	0	0	1	1	0	0	1	1	0	0	0	0	0	1	1
0	0	1	1	1	0	0	0	0	1	0	0	0	1	1	0	0	1	1	0	1
0	0	1	1	1	0	0	0	1	1	0	0	0	0	0	0	1	1	0	0	0
1	1	1	1	1	1	0	0	1	1	0	0	0	0	0	1	1	0	0	0	0
1	1	0	0	1	1	0	0	0	0	0	0	0	0	1	1	1	0	0	0	0
1	0	0	0	1	1	0	0	1	0	0	1	1	0	1	1	1	0	0	0	0
0	0	0	0	0	0	0	0	0	0	0	0	0	0	1	1	0	0	0	0	0
0	0	0	0	0	0	0	0	0	1	1	0	0	1	1	1	0	0	1	0	0
0	0	0	0	0	0	0	0	0	0	1	0	0	0	1	1	1	1	1	0	0
0	0	0	0	0	1	0	0	0	0	0	1	0	0	1	1	1	1	1	1	0
0	0	0	0	0	1	0	0	0	0	0	1	1	0	0	0	0	0	1	0	0
0	0	0	0	0	0	0	0	0	0	0	1	1	0	1	0	0	1	1	0	0
0	0	0	0	0	0	0	0	0	0	0	1	1	1	1	0	0	0	0	0	0
0	0	0	0	0	0	0	0	0	0	0	1	1	1	1	1	1	0	0	0	0	0
0	0	0	0	0	0	0	0	0	0	0	0	1	1	1	1	0	0	0	0	0	0
0	0	0	0	0	0	0	0	0	0	0	0	0	1	1	1	0	0	0	0	0	0
0	0	0	0	0	0	0	0	0	0	0	0	0	0	0	0	0	0	0	0	0	0

Figure 3.10 – Pixel values for binary metaphase window

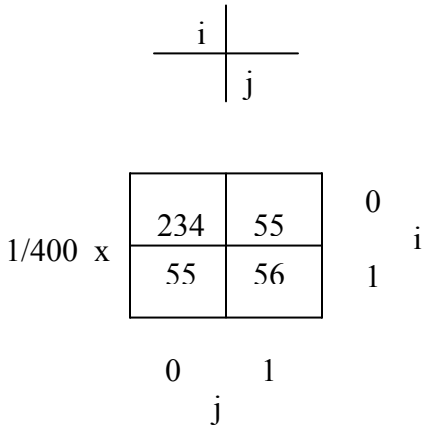


Figure 3.11 – Co-occurrence matrix for **d** = (1,1).

If we apply the counting process to the values in Figure 3.10, we get the values in the matrix as shown. What the matrix values show, is that by far the most

common pairing is the (0,0) combination. The other three combinations are about equal, with each about 14% of the total.

The feature values are then calculated as follows:

$$\text{Entropy} = -\Sigma\,\Sigma\, P[i,j] \log P[i,j] = 0.493.$$

$$\text{Energy} = \Sigma\,\Sigma\, P^2[i,j] = 0.399.$$

$$\text{Contrast} = \Sigma\,\Sigma\, (i-j)^2\, P[i,j] = 0.275.$$

$$\text{Homogeneity} = \Sigma\,\Sigma\, P[i,j] / (1+|i-j|) = 0.863.$$

Some characteristics of these features are worth mentioning. First, the entropy is a measure of how dissimilar and random the pixel values are. A high value of entropy then says that the one-pixels are more randomly distributed. The energy value tells to what extent the pairings tend to be of just one type. The contrast is a measure of how different the neighboring pixels are. It should be noted that, for the 2 x 2 matrix, with **d** = (1,1), the contrast value depends only on the off-diagonal sums. Homogeneity is a summation of the pixels, weighted to favor the on-diagonal elements. It is somewhat the opposite of contrast. It is a measure of the size of the all-white and all-black regions within the texture.

Effective limits for the feature values were determined experimentally as follows:

Entropy: 0.38 - 0.63

Energy: < 0.5

Contrast: > 0.15

Homogeneity: < 0.9

As one would expect, making the limits wider will identify more metaphases, but at the cost of causing more false positive. On the other hand, tightening the limits will result in more false negatives.

The value of **d** is usually chosen by experiment, and a texture may be tested with more than one value of **d**, just as it may be tested with more than one type of gray-level. For metaphase finding, a 2x2 matrix proved to be just as effective as a 3x3, and is faster to compute. Also, the choice of **d** did not significantly affect the results of our tests, so the simple (1,1) value was chosen as the standard.

As an illustration of the way the metaphase finder works on a scanned image, a frame of a scan was chosen to test the finder. Figure 3.13 shows the results of running the metaphase finder on a still image with 10X objective power . Figure 3.12 is the original still image which contains four candidate metaphases, while Figure 3.13 shows the results output from the finder. The finder shows the metaphases in reverse image and the XY coordinates of them are available as an output. Two of the metaphases were correctly identified, while two were missed due to being excessively spread out, and one false positive occurred on a piece of debris. Figure 3.14 is the blurred image of the same slide region scanned at 1 mm/sec, and Figure 3.15 shows that the metaphase finder achieved the exact same result as with the still image. The false positive on the piece of debris could be eliminated with an additional feature measurement, such as shape or size.

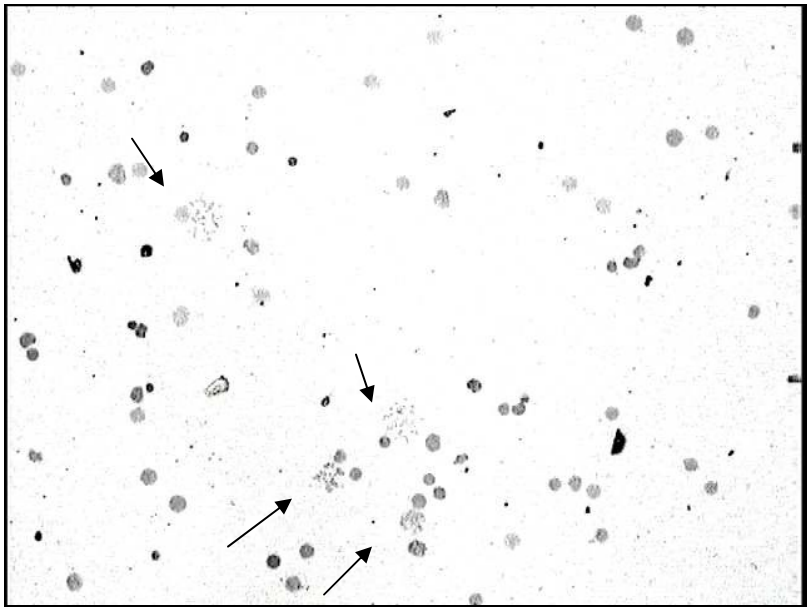


Figure 3.12 – Still image containing four candidate metaphases.

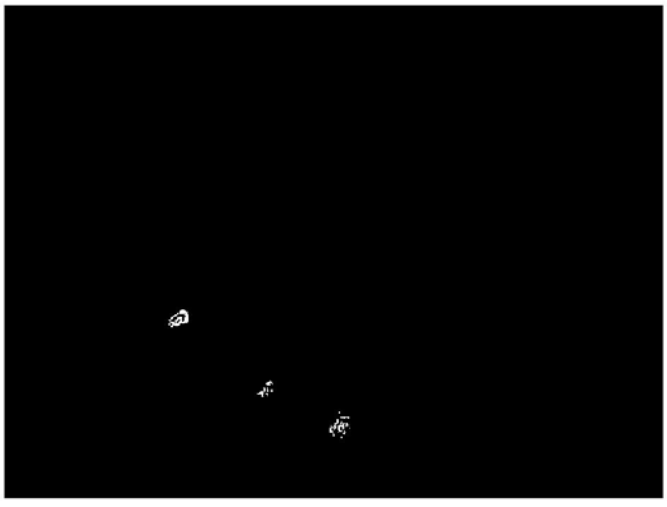


Figure 3.13 – Result of metaphase finder process.

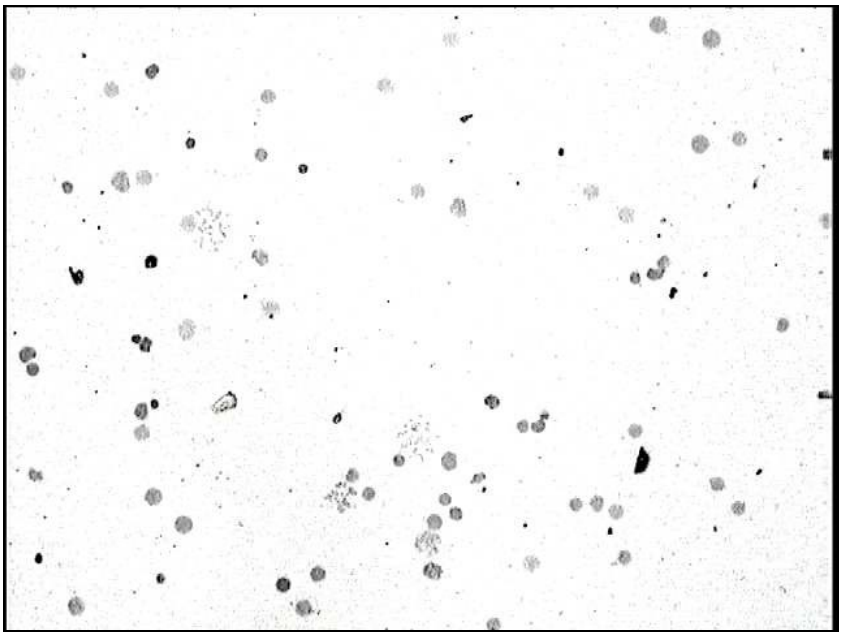


Figure 3.14 – Scan image of same tissue area.



Figure 3.15 – Results of finder process.

Section 3.3 – Stage Coordinate Repeatability

Another important feature of the scanning system is the repeatability of stage positioning. In order for the system to be easy to use, a user should be able to command the stage to return to the exact coordinates of a chosen metaphase. Therefore, a test of this ability was performed. The test consisted of choosing a metaphase near an edge of the tissue area, capturing the image using the 60X lens, and recording its XY coordinates (by sending the "where XY" command to the controller). Then, the stage was commanded to move to some other location, in this case the 0,0 "home" position, and then immediately commanded to return to the metaphase coordinates, where the image was re-captured. This trip was repeated four times. Figure 3.16 shows the captured images. The metaphase is in the approximate center of the viewing area in each case, ensuring that a human user will be able to easily find and reexamine any chosen metaphase at a later time. The diameter of this metaphase is approximately 30 μm.

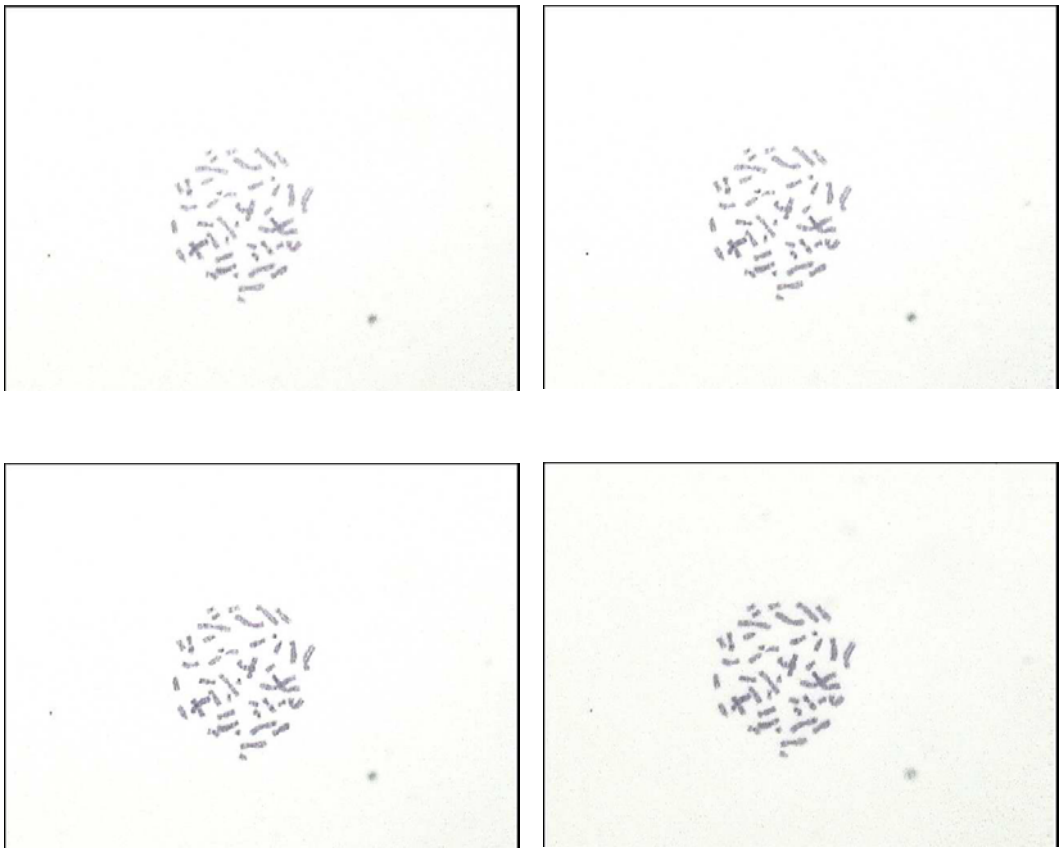


Fig. 3.16 – Metaphase repeatedly located by software command.

Section 3.4 – Summary

The results of these experiments have established that a simple texture-based metaphase finder is effective for motion scans up to a 1mm/sec rate and 10X objective power. Though the MTF of the system is reduced as the scan rate increases, the salient features of the metaphase texture are sufficiently preserved to allow efficient finding at moderate scan rates. Since our simple texture based method produces such reliable results, a more sophisticated algorithm should be able to identify metaphases with an even higher degree of accuracy. The motorized stage was shown to have sufficient accuracy to report the position of a metaphase and to

subsequently return to that position within a few microns of the original position. This capability is essential if the results of the metaphase finder are to be effectively used by subsequent operations, such as metaphase scoring and high magnification image capture.

Chapter IV – Conclusion

The results of this research indicated that image quality is one of the most important features that a scanning system must have to be effective. The quality is determined by the components in the optical/video path, how the components are adjusted, and the scanning speed. The Modulation Transfer Function (MTF) is a useful way of quantifying the image quality. Each component in the system will have its own value of MTF and the overall system MTF is found by multiplying the individual MTFs together. Motion blur will reduce the MTF even further, so scanning speed is limited by the deterioration of the image features. Motion blur is worse for higher levels of magnification, causing the MTF to drop off rapidly as the spatial frequencies increase. This is true because a higher level of magnification produces a smaller field of view, and so more image pixels pass under a CCD pixel element during each frame. One solution is to image a slide in a "tile" method, where the stage moves in a start-stop motion for each frame. This idea reduces motion blur, but requires significantly more scan time and causes detrimental wear and tear on the stage motors and gears.

Scanning with a 10X objective lens allows for efficient processing and accurate metaphase finding. MTF values drop off quickly as scan speed and magnification level increases, but the essential texture of a metaphase spread can still be recognized for 10X magnification and moderate scan speed. A camera with a pixel size of approximately 3.5 μm, using 10X objective power, will provide enough resolution to preserve the metaphase features. A scan can be completed in 15 minutes

with a scan speed of about 1 mm/sec. The texture-based method of metaphase recognition works well enough to provide an acceptable level of accuracy.

Future research will include Phase II of the project, where the image processing and karyotyping algorithms will be integrated with the hardware and control software. Improvements in the hardware include obtaining a dry 100X lens, so that high resolution images of chromosomes can be made automatically, without a user needing to be present to apply oil to the slide. The system design principles and algorithm development originating from this research may facilitate the development of a Computer Aided Diagnosis (CAD) based automated scanning system for routine clinical use.

REFERENCES

1. K.R. Castleman, "Match Recognition In Chromosome Band Structure," *Biomed. Sci. Instrum.* 4:256-64, 1968.

2. K.R**.** Castleman, "Computers and Chromosomes", S.W. Wright, B.F. Crandall and L. Boyer, Eds. *Perspectives in Cytogenetics: The Next Decade*, Charles C. Thomas, Springfield, 1970.

3. T.J. Golab, "MACDAC - An Inexpensive and Complete Biomedical Input and Output Display System", Proc. 23rd ACEMB, Nov. 1970.

4. E. Patrick, et al, "Computer Controlled Picture Scanning with Application to Labeled Biological Cells", Comput. Biol. Med. 1972, vol. 2, No. 1, pp. 5-14.

5. K.R. Castleman, and R.J. Wall, "Automatic Systems for Chromosome Identification", *Nobel* **23**:77-84, 1973.

6. D. Greenand, and P. Neurath, 'The Design, Operation and Evaluation of a High Speed Automatic Metaphase Finding Algorithm",*J. Histochem. Cytochem.*,**22**, 1974, pp. 531–535.

7. K.R Castleman, et al, "Automated Clinical System for Chromosome Analysis", United States Patent 4,122,518, October 24, 1978.

8. J. Piper, "Automation of Chromosome Analysis", *Signal Processing,* 1980.

9. P. Nickolls, and J. Piper, "Pre-processing of Images in an Automated Chromosome Analysis System", *Pattern Recognition,* 1981.

10. K.R Castleman**,** et al, "A Pipeline Multiprocessor Architecture for High Speed Cell Image Analysis" *IEEE-CAPAIDM*, 52-54, 1983.

11. C. Lundsteen, "Automatic Classification of Chromosomes as Part of a Routine System for Clinical Analysis", *Cytometry*, 1986.

12. J. Graham, and D. Pycock, "Automation of Routine Clinical Chromosome Analysis: I – Metaphase Finding", *Analytical and Quantitative Cytology and Histology*, 1987.

13. J. Graham, and D. Pycock, "Automation of Routine Clinical Chromosome Analysis: II – Chromosome Analysis", *Analytical and Quantitative Cytology and Histology*, 1987.

14. L. van Vliet, et al, "Athena Macintosh Karyotyping System", *Automation of Cytogenetics,* 1989.

15. J. Piper and E. Granum, "On Fully Automatic Feature Measurement", *Cytometry*, 1989.

16. J. Piper, "Automatic Detection of the X Chromosome", *Cytometry*, 1990.

17. Q. Wu, P. Suetens, and A. Oosterlinck, "Chromosome Classification Using a Multi-layer Perceptron Neural Net", Proc. 12th annual Int. Conf. IEEE Engineering in Medicine and Biology Society, vol 3, 1990, pp 2249-52.

18. L. Vanderheydt, F.Dom, A. Oosterlinck, and H Befghe, "Two-dimensional Shape Decomposition Using Fuzzy Subset Theory Applied to Automated Chromosome Analysis", *Pattern Recognition* **13**, 1981, pp 147-57.

19. K. R. Castleman, and D. Fabian, "User Interface Design for a General Purpose Pattern Recognition Package," *SPIE* **755**: 114-125, 1987.

20. B. Mayall, "Experience with the Athena Semi-Automatic Karyotyping System", *Cytometry*, 1990.
21. A. Carothers, and J. Piper, "Computer-aided Classification of Human Chromosomes: A Review", *Statistics and Computing*, 1994, pp161-171.
22. M. Popescu, et al, "Automatic Karyotyping of Metaphase Cells With Overlapping Chromosomes", *Computers in Biological Medicine*, 1998.
23. L. Alvarado, "Inter-chromosome Texture", *Medical and Biological Engineeering and Computation*, 2002.
24. M. Akbari, "Improving the Automatic Karyotyping Accuracy of the Chromosome Features Using Fuzzy Logic", *IEEE*, 2004.
25. P. Biyani, "Globally Optimal Classification and Pairing of Human Chromosomes, *IEEE EMBS Proceedings"*, 2004.
26. X. Wang, B. Zheng, M. Wood, S. Li, W. R. Chen, and H. Liu, "Development and Evaluation of Automated Systems for Detection and Classification of Banded Chromosomes: Current Status and Future Perspectives", *Journal of Physics D: Applied Physics*, 2005.
27. X. Wang, S.Li, H. Liu, M. Wood, W. R. Chen, and B. Zheng, "Automated Identification of Analyzable Metaphase Chromosomes Depicted on Microscopic Digital Images", *Journal of Biomedical Informatics*, 2007.
28. Aperio, Inc, "Precise Motion Control Contributes to Virtual Microscopy", www.Aperio.com, 2006.
29. Metasystems GmbH, "Ikaros Karyotyping System", *www.metasystems.de,* 2006.
30. Imstar, "Fast Metphase Finder", *www.imstar.fr,* 2006.
31. B. Czepulkowski, *Analyzing Chromosomes*, Springer-Verlag, New York, 2001.
32. R.S. Verma and A. Babu, *Human Chromosomes Principles and Techniques*, Second Edition, McGraw-Hill, 1995.
33. D. S. Nicholl, *An Introduction to Genetic Engineering*, Cambridge University Press, Cambridge, 2000.
34. A. J. Griffiths, J.H. Miller, and D.T. Suzuki, *An Introduction to Genetic Analysis, Seventh Edition*, W.H. Freeman, New York, 2000.
35. B. R. Glick and J. J. Paternak, *Molecular Biotechnology*, Second Edition, ASM Press, Washington, D.C., 1998.
36. D. B. Murphy, *Fundamentals of Light Microscopy and Electronic Imaging*, Wiley-Liss, New York, 2001.
37. S. Inoue and K. R. Spring, *Video Microscopy, The Fundamentals, Second Edition*, Plenum Press, New York, 1997.
38. U. Catalyurek, M. D. Bynon, C. Chang, T. Kurc, A. Sussman, and J. Saltz, "The Virtual Microscope", IEEE Transactions on Information Technology in Biomedicine, 2001, pp. 230-248.
39. J. T. Bushberg, J. A. Seibert, E. M. Leidholdt, and J. M. Boone, *The Essential Physics of Medical Imaging, Second Edition*, Lippincott Williams & Wilkins, Philadelphia, 2002.
40. E. Hecht, *Optics, Fourth Edition*, Addison Wesley, New York, 2002.
41. T. Kenjo and A. Sugawara, *Stepping Motors and Their Microprocessor Controls, Second Edition*, Clarendon Press, Oxford, 1994.

42. W. H. Yeadon, and A.W. Yeadon, *Handbook of Small Electric Motors*, McGraw Hill, New York, 2001.
43. R. Jain, R. Kasturi, and B. B. Schunk, *Machine Vision*, McGraw-Hill, New York, 1995.
44. A. Bovik, Ed., *Handbook of Image & Video Processing*, Academic Press, San Diego, 2000.
45. C. Pun, "Rotation-Invariant Texture Feature for Image Retrieval", *Computer Vision and Image Understanding*, 2003, pp. 24-41.
46. S. Bow, *Pattern Recognition and Image Processing, Second Edition*, Marcel Dekker, New York, 2002.
47. A. Webb, *Statisitical Pattern Recognition, Second Edition*, John Wiley & Sons, Chichester, 2002.
48. R.O. Duda, P.E. Hart, and D.G. Stork, *Pattern Classification, Second Edition*, John Wiley & Sons, New York, 2001.
49. C.H. Chen and P.S.P. Wang, *Handbook of Pattern Recognition and Computer Vision*, Third Edition, World Scientific, London, 2005.
50. J. P. Havlicek, "The Evolution of Modern Texture Processing", *Electrik*, The Scientific and Technical Research Council of Turkey, Istanbul, 1997, pp. 1-29.
51. H. K. Huang, *PACS and Imaging Informatics*, Wiley-Liss, Hoboken, 2004.